



# **Transonic Wing/Store Flow-Field Measurement Using a Laser Velocimeter**

**F. L. Heltsley, F. L. Crosswy,  
and D. Brayton  
ARO, Inc.**

**August 1981**

**Final Report for Period March 8, 1979 -- September 30, 1980**

Approved for public release; distribution unlimited.

**ARNOLD ENGINEERING DEVELOPMENT CENTER  
ARNOLD AIR FORCE STATION, TENNESSEE  
AIR FORCE SYSTEMS COMMAND  
UNITED STATES AIR FORCE**

## NOTICES

When U. S. Government drawings, specifications, or other data are used for any purpose other than a definitely related Government procurement operation, the Government thereby incurs no responsibility nor any obligation whatsoever, and the fact that the Government may have formulated, furnished, or in any way supplied the said drawings, specifications, or other data, is not to be regarded by implication or otherwise, or in any manner licensing the holder or any other person or corporation, or conveying any rights or permission to manufacture, use, or sell any patented invention that may in any way be related thereto.

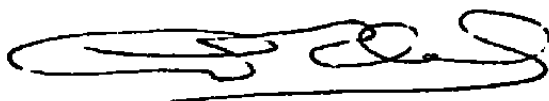
Qualified users may obtain copies of this report from the Defense Technical Information Center.

References to named commercial products in this report are not to be considered in any sense as an indorsement of the product by the United States Air Force or the Government.

This report has been reviewed by the Office of Public Affairs (PA) and is releasable to the National Technical Information Service (NTIS). At NTIS, it will be available to the general public, including foreign nations.

## APPROVAL STATEMENT

This report has been reviewed and approved.



ALVIN R. OBAL, Captain, CF  
Directorate of Technology  
Deputy for Operations

Approved for publication:

FOR THE COMMANDER



MARION L. LASTER  
Director of Technology  
Deputy for Operations

# UNCLASSIFIED

REPORT DOCUMENTATION PAGE		READ INSTRUCTIONS BEFORE COMPLETING FORM
1 REPORT NUMBER <b>AEDC-TR-80-54</b>	2 GOVT ACCESSION NO.	3 RECIPIENT'S CATALOG NUMBER
4 TITLE (and Subtitle) <b>TRANSONIC WING/STORE FLOW-FIELD MEASURE- MENT USING A LASER VELOCIMETER</b>		5 TYPE OF REPORT & PERIOD COVERED <b>Final Report-March 8, 1979 to September 30, 1980</b>
		6. PERFORMING ORG. REPORT NUMBER
7 AUTHOR(s) <b>F. L. Heltsley, F. L. Crosswy, and D. Brayton, ARO, Inc., a Sverdrup Corporation Company</b>		8 CONTRACT OR GRANT NUMBER(s)
9 PERFORMING ORGANIZATION NAME AND ADDRESS <b>Arnold Engineering Development Center/DOT Air Force Systems Command Arnold Air Force Station, Tennessee 37389</b>		10 PROGRAM ELEMENT, PROJECT, TASK AREA & WORK UNIT NUMBERS <b>Program Element 61102F</b>
11 CONTROLLING OFFICE NAME AND ADDRESS <b>Arnold Engineering Development Center/DOS Air Force Systems Command Arnold Air Force Station, Tennessee 37389</b>		12. REPORT DATE <b>August 1981</b>
		13. NUMBER OF PAGES <b>55</b>
14 MONITORING AGENCY NAME & ADDRESS (if different from Controlling Office)		15 SECURITY CLASS. (of this report)  <b>UNCLASSIFIED</b>
		15a DECLASSIFICATION/DOWNGRADING SCHEDULE <b>N/A</b>
16 DISTRIBUTION STATEMENT (of this Report)  <b>Approved for public release; distribution unlimited.</b>		
17 DISTRIBUTION STATEMENT (of the abstract entered in Block 20, if different from Report)		
18 SUPPLEMENTARY NOTES  <b>Available in Defense Technical Information Center (DTIC)</b>		
19 KEY WORDS (Continue on reverse side if necessary and identify by block number) <b>wind tunnel tests      stores measurements          models flow fields              velocity configurations          laser velocimeters wings</b>		
20 ABSTRACT (Continue on reverse side if necessary and identify by block number)  <b>A test was conducted in the Arnold Engineering Development Center (AEDC) Aerodynamic Wind Tunnel (1T) of the Propulsion Wind Tunnel Facility (PWT) to measure the flow fields about several wing/pylon/store configurations. Test models included a wall- mounted swept wing, five-percent MK-83 and M-117 stores, and swept and unswept pylons. Flow-field velocity measurements, made by using a three-component laser velocimeter, are presented.</b>		

# UNCLASSIFIED

## **PREFACE**

The work reported herein was conducted by the Arnold Engineering Development Center (AEDC), Air Force Systems Command (AFSC), at the request of the Air Force Armament Laboratory (AFATL/DLJC), AFSC. The AFATL project manager was Dr. Lawrence Lijewski. The AEDC project manager was Capt. Alvin R. Obal (CF). The results were obtained by ARO, Inc., AEDC Group (a Sverdrup Corporation Company), operating contractor for the AEDC, AFSC, Arnold Air Force Station, Tennessee, under ARO Project No. P34E-42. The manuscript was submitted for publication on September 30, 1980.

Messrs. Heltsley, Crosswy, and Brayton are currently employed by Calspan Field Services, Inc., AEDC Division.

## CONTENTS

	<u>Page</u>
1.0 INTRODUCTION .....	5
2.0 APPARATUS	
2.1 Test Facility .....	5
2.2 Test Articles .....	6
2.3 Instrumentation .....	6
2.4 Fluidized Bed Particle Seeder .....	6
3.0 PROCEDURE	
3.1 Test Conditions .....	7
3.2 Laser Velocimeter Data Acquisition .....	7
3.3 Data Reduction .....	7
3.4 Precision of Measurements .....	9
4.0 RESULTS AND DISCUSSION .....	11
5.0 CONCLUDING REMARKS .....	11
REFERENCES .....	11

## ILLUSTRATIONS

### Figure

1. Tunnel 1T Layout and LV System Installation .....	13
2. Model Dimensions .....	14
3. Configuration Identification .....	17
4. Coordinate System Definition .....	18
5. Basic Wing/Pylon/Store Configurations .....	19
6. Tunnel 1T Three-Velocity Component LV Optical System Installation .....	20
7. LV Data Acquisition System Schematic .....	21
8. Offline Data Processing Sequence .....	22
9. Configuration 221 Installed in Tunnel 1T with the Three-Component LV Beams Passing through the Gap between the Pylon and Store .....	23
10. Mean Velocity Vector Projections in Constant x Planes for Configuration 111 ( $\alpha_w = 0$ ), $M_\infty = 0.92$ .....	24
11. Effect of Pylon on Mean Velocity Vector Projections in Constant z Plane for Two Wing/MK-83 Configurations ( $\alpha_w = 2.0$ ), $M_\infty = 0.92$ , $z/D = 0.56$ .....	28

FigurePage

12. Effects of Pylon on Velocity Vector Projections in Constant z Plane for Four Wing/MK-83 Configurations ( $\alpha_w = 0$ ), $M_\infty = 0.920$ , $z/D = 0.56$ .....	30
13. Effect of Mach Number on Mean Velocity Vector Projections in Constant z Plane for Configuration 121, $z/D = 0.56$ .....	34
14. Effect of Pylon on Mean Velocity Vector Projections in Constant y Plane for Three Wing/MK-83 Configurations ( $\alpha_w = 0$ ), $M_\infty = 0.92$ , $y/D = 0$ .....	36
15. Effect of Pylon on Velocity Vector Projections in Constant y Plane for Two Wing/M-117 Configurations ( $\alpha_w = 2.0$ ), $M_\infty = 0.92$ , $y/D = 0$ .....	39
16. Distribution of the Mean Velocity Components Along the x Axis (Store Centerline) with the Store Removed, $M_\infty = 0.92$ , Configurations 200, 210, and 220 .....	41
17. Effect of Wing Angle on the Distribution of Mean Velocity Magnitude between the Wing and Store, $M_\infty = 0.92$ , $y/D = 0$ .....	42
18. Wing Boundary-Layer Characteristics on Configuration 100 Lower Surface, $M_\infty = 0.92$ .....	43

**TABLE**

1. Test Conditions .....	45
--------------------------	----

**APPENDIXES**

A. Laser Doppler Velocimeter System Details .....	47
B. Resolution of the y Component of Velocity .....	49
C. Uncertainty in the y Component of Velocity .....	51

NOMENCLATURE .....	53
--------------------	----

## **1.0 INTRODUCTION**

The interference flow field about a store-laden aircraft is frequently the most important parameter affecting a store trajectory. Lack of accurate experimental data has been a major hindrance to development and evaluation of analytical techniques for computing such flows, especially in the transonic regime. The occurrence of shock waves within the flow field, often accompanied by regions of flow instability, makes measurement by conventional mechanical probes unreliable. A nonperturbing device such as a laser Doppler velocimeter (LV) must be used if accurate velocity measurements are to be obtained throughout a transonic flow field.

The purpose of this investigation was to obtain LV measurements in the flow fields of several wing/pylon/store configurations. The flow-field surveys were conducted with use of a three-component LV system in the Arnold Engineering Development Center (AEDC) Aerodynamic Wind Tunnel (1T) of the Propulsion Wind Tunnel (PWT) Facility.

## **2.0 APPARATUS**

### **2.1 TEST FACILITY**

The AEDC Tunnel 1T is a continuous-flow, open-circuit wind tunnel that can be operated over a Mach number range from 0.20 to 1.50. The tunnel operates at a constant stagnation pressure of approximately 2,850 psfa. Stagnation temperature in the tunnel can be varied from 80 to 120°F above ambient temperature. A complete description of the facility is included in Ref. 1.

The four test section walls used during the test were 6-percent perforated except for a closed region on either sidewall extending from Sta 14.6 to Sta 26.6. Optical-quality windows were installed in the plenum and test section sidewalls adjacent to the LV. A variable angle-of-attack wing mount was located between the same tunnel stations on the opposite test section wall. The plenum window was mounted in a special inset assembly that allowed positioning it close to the tunnel window. The arrangement permitted the LV beam array to be traversed about the test article without requiring a large, prohibitively expensive plenum window. A plan view of the Tunnel 1T test area showing the LV system installation is presented in Fig. 1. The fluidized bed particle seeder shown exhausting into the air intake room was utilized to supplement the ambient atmospheric particles and, thus, to improve the data acquisition rate.

## 2.2 TEST ARTICLES

Test hardware included a wall-mounted 45-deg swept wing with a constant 6-in. chord NACA 0005-34 airfoil cross section, two 1/20-scale store models (an MK-83 and an M-117), and two pylons, one with unswept and the other with 60-deg swept leading and trailing edges. Model dimensions are presented in Fig. 2. The configuration identification and coordinate system are given in Figs. 3 and 4, respectively.

Fourteen test configurations were investigated. The configurations, defined in Table 1, are all variations of the five basic wing/pylon/store combinations shown in Fig. 5.

## 2.3 INSTRUMENTATION

The standard tunnel system was used to record the test conditions and model pressures. The flow-field measurement utilized a three-velocity component LV system. Figure 6 shows the optical arrangement of the LV. The system consisted basically of both a two-component LV and a single-component LV mounted on the same traverse table and sharing a common laser light source. A blue beam, two-component LV provided the magnitude of the velocity components parallel to the x and z axes of the mutually orthogonal wind tunnel coordinate system. Rather than measuring the component magnitude parallel to the y axis directly, a green beam, single-component LV obtained the velocity component in the y' direction. A more detailed description of the system is contained in Appendix A. The technique for resolving the y component of velocity from the measured components is described in Appendix B and Ref. 3.

## 2.4 FLUIDIZED BED PARTICLE SEEDER

The tunnel flow was seeded with alumina particles with a nominal diameter of one micron. As shown in Fig. 1, the seed particles were introduced into the air intake room along with atmospheric particles. These particles then passed through the intake filters and the compressor, which tended to remove the larger particles and break up clustered seed particles. Under unseeded conditions the time required to record an LV data point varied from several seconds to several tens of seconds depending upon the atmospheric dust content. Operation of the seeder reduced this time by approximately 50 percent. It is important to emphasize that the amount of seed material required was minimal: Less than three pounds of alumina powder were used during several hundred hours of testing. Neither the tunnel nor model, apparently, suffered any adverse effects.



### 3.0 PROCEDURE

#### 3.1 TEST CONDITIONS

The test was designed to investigate the mutual interference between components of each configuration in the transonic Mach number range. As shown in Table 1 each configuration was tested at  $M_\infty = 0.920$ , which was determined experimentally (Ref. 2) as the lowest Mach number for which a shock was firmly established between the store and the wing lower surface of Configuration 201. In addition, selected configurations were tested at  $M_\infty = 0.975$  and/or 1.025. During the tests, a tunnel stagnation temperature of 160°F was maintained to minimize velocity continuity errors.

#### 3.2 DATA ACQUISITION

The LV data were recorded by a computer-based data acquisition system shown in block diagram form in Fig. 7. Nominally 1,000 velocity samples were recorded for each of the velocity components at each point of interest in the flow field. The time required to record these data varied from several seconds to several tens of seconds, depending upon the atmospheric dust content of the intake air. A more desirable and controllable rate of data acquisition was obtained by using the seeder.

The terminal shown in Fig. 7 provided an online view of the LV velocity data and the free-stream tunnel velocity derived from tunnel pressure and temperature measurements. The printer provided a hard copy of these CRT data while the magnetic tape unit was the primary means for recording data.

The focal volume position relative to the test model was recorded for each velocity data set. Periodic corrections were necessary, however, to minimize spatial error caused by temperature effects.

#### 3.3 DATA REDUCTION

A generalized LV data reduction and analysis software package has been developed that can process up to three components of either nonsimultaneous or simultaneous velocity data. The program provides for extensive statistical analysis, including computations of sample statistics and estimations of population parameter values. The quantities computed include mean, variance, standard deviation, third and fourth moment, skewness, kurtosis, and absolute deviation as defined in Ref. 4. The mode of each sample distribution can also be determined independent of the performance of "split" statistical computations on the

portions of the distribution on either side of the mode value. For nonsimultaneous data, the component means and modes can be transformed from LV measurement coordinates into any desired mutually orthogonal axis system and the total mean and mode velocity vector magnitudes can also be calculated (Appendix B). For simultaneous data sets, the coordinate transformation can be performed on the discrete particle velocity component sets before the statistical analyses. The correlation provided by the simultaneity condition also permits the computation of several additional statistical parameters including covariances (Reynolds shear stresses), correlation coefficients, the generalized variance, and the scatter coefficient (Ref. 4).

A master summary file containing the results of the various data reduction procedures can be accessed for printing or plotting output or for further analysis. A diagram of the offline data processing sequence is presented in Fig. 8.

### **3.4 PRECISION OF MEASUREMENTS**

#### **3.4.1 Tunnel Conditions**

Care was taken to allow the tunnel to stabilize before the relatively long data-recording period. The resulting variation in mean free-stream Mach number was estimated to be  $\pm 0.003$ . The variation in mean free-stream velocity was less than  $\pm 5.0$  ft/sec. The sidewalls with windows presented an additional source of Mach number uncertainty. According to the Tunnel 1T calibration (Ref. 5), use of the windows can result in significant variation in Mach number along the tunnel centerline. A statistical analysis of the centerline Mach number resulted in a  $2\text{-}\sigma$  deviation from the mean free-stream Mach number of  $\pm 0.035$ .

#### **3.4.2 Spatial Resolution**

The LV probe volume was positioned in the test article flow field by moving, as a unit, the laser and optical components shown on the traverse table in Fig. 6. The traverse system could be programmed to step in integer multiples of 0.001 in. in the x- and y-axis directions and in integer multiples of 0.00038 in. in the z-axis direction. The tip of the store model served as the origin of the x-y-z tunnel reference coordinates. Because of thermal expansion effects, this origin moved as a function of elapsed tunnel run time. Therefore, it was necessary to relocate the model tip periodically by observing the precisely repeatable diffraction patterns by the transmitted laser beams, contacting the tip and upper and lower surfaces of the store model. The repeatability of the model tip position determinations was within  $\pm 0.010$  in. for the x and z axes.

A velocity scan was the means to determine the lateral (y) position of the model. Laser velocity data were recorded at from 15 to 20 points along a constant y-z line from one side of the model to the other in the region of high-velocity gradient near the model nose. The actual model centerline position could usually be determined to within  $\pm 0.030$  in. from the symmetry of the velocity distribution in the y direction. The technique is suitable for most models symmetrical about a constant y plane. The results are valid at any angle of attack as long as the yaw angle remains small; this angle is critical because an error in yaw caused by tunnel flow angularity or model misalignment can destroy the symmetry of the upward velocity distribution, resulting in a larger y-position uncertainty. It should be noted that all the  $V_y$  distributions observed in the present test were acceptably symmetrical.

### 3.4.3 Laser Velocimeter Measurements

The velocity measurements in the x, y', and z directions were usually repeatable to within  $\pm 10.0$  ft/sec. This corresponds to the relative uncertainties of  $\pm 1.0$  and  $\pm 1.2$  percent in the  $V_{ux}$  and  $V_y$  components, respectively, at  $M_\infty = 0.92$ . The uncertainty in the resolved  $V_y$  component was found to be somewhat higher than that observed in the components measured directly. The error sources are discussed in Appendix C.

## 4.0 RESULTS AND DISCUSSION

LV velocity measurements were made for each test configuration at the same predetermined survey points in the vicinity of the test article. The particular points were selected to provide optimum flow-field definition and to assess mutual aerodynamic interference between the model elements. Several of the survey grid points were located on the opposite side of the pylon from the LV system and required measurement either through the transparent pylon or through the gap between the pylon and store (Fig. 9). All survey point coordinates are referenced to the store nose as illustrated in Fig. 4.

Velocity vector projections measured in several constant x planes are presented in Fig. 10 for Configuration 111. Figures 10c and d contain examples of measurements taken through the pylon and measurements obtained through the pylon/store gap.

The vector projections of velocities measured in a constant z plane passing through the pylon/store gap are presented in Figs. 11 through 13. Figures 11 and 12 show that the unswept pylon causes more severe flow-field disturbances in the forward region than does the swept pylon; the figures also show that larger sidewash angles occur beneath the aft portion of the pylon for a wing angle of attack of zero (Configurations 121 and 111). The sidewash disturbance is stronger at a wing angle of attack of 2.0 deg, however, for the unswept pylon (Configuration 221).

Mach number effects on the Configuration 121 flow field can be seen in Figs. 12b and 13. Although stronger sidewash appears near the pylon at  $M_\infty = 0.92$  than at  $M_\infty = 0.975$ , the subsonic flow fields are quite similar at  $z/D = 0.56$ . The supersonic case, shown in Fig. 13b, produced a general outward flow tending toward the wing tip.

The effect of pylons upon flow-field velocity vectors measured in a constant  $y$  plane are presented in Figs. 14 and 15 for the MK-83 and M-117 store, respectively, with the wing at zero deg angle of attack. Except for the differences in vector angle and magnitude near the pylon leading edge, the MK-83 flow fields appear to be nearly identical. Likewise, the M-117 configurations exhibit only minimal differences in the selected constant  $y$  plane. The gradients are generally larger for the M-117 than for the MK-83 configurations.

Distributions of the three orthogonal components of velocity measured "along a line where the centerline of the store would be if it were installed" (Ref. 6) are presented in Fig. 16 for the three configurations with a wing angle of attack of 2.0 deg. Such data could be used for computing initial or launch conditions for a store using the flow angularity techniques described in Refs. 6 and 7. As previously observed, the unswept pylon generates larger flow field disturbances than does the swept pylon.

In addition to obtaining the flow-field grid data, more detailed surveys were made for selected configurations to detect the presence and location of embedded shock waves. The results of three such surveys (Fig. 17) illustrate the effect of wing angle of attack on the shock characteristics of Configurations 101 and 201. The velocity distributions at  $z/D = 0.74$  reveal what appears to be a secondary weak shock at approximately  $z/D = 4.0$  in the Configuration 101 flow field; this shock is not present for Configuration 201. A survey closer to the store at  $z/D = 0.56$  confirmed the existence of one and possibly two additional shock-like disturbances forward of the strong primary shock at  $x/D = 5.7$ . The velocity distribution immediately downstream of the Configuration 201 shock is essentially the same as that observed previously in the two-component LV investigation (Ref. 2), indicating that similar errors from particle dynamics were present. Discussions of the so-called "particle lag" effect can be found in Refs. 2 and 8.

The LV boundary-layer profiles described in Fig. 18 were obtained along a constant  $x$ - $y$  line beneath the wing of Configuration 100 at the 40-percent chord point. The results are plotted against the local normal coordinate,  $z_s/\delta$ , which is positive away from the surface and nondimensionalized by an estimated boundary-layer thickness of 0.16 in. The large values of  $(y/V_E)$  and  $[(V_x/V_y)_{ME}/V_E^2]$  which occur in the profiles at  $(z_s/\delta) > 1.0$  are not consistent with the assumption of isotropic turbulence outside the boundary layer; these large values are probably caused by the  $y$ -component uncertainty discussed in Appendix C.

If the higher-order statistical information presented in Figs. 18b and 18c is of primary interest, the LV measurement coordinate system should be optimized to minimize y-component resolution uncertainty.

## 5.0 CONCLUDING REMARKS

The transonic flow fields of several wing/pylon/store configurations were investigated by using a three-velocity-component LV. The results indicate that an LV can provide useful nonintrusive velocity measurements for such applications.

The representative examples of the experimental data presented reveal the flow field to be rather complex in contrast to the relative simplicity of the model. As a rule, the unswept pylon generated larger disturbances than did the swept one. Larger flow deflections were observed for the M-117 store than were observed for the less blunt MK-83. The disturbance that occurred near the lower pylon leading edge was intensified by the presence of the store.

The present investigation marked the first use of a three-component LV at the AEDC.

## REFERENCES

1. *Test Facility Handbook* (Eleventh Edition). "Propulsion Wind Tunnel Facility, Vol. 4." Arnold Engineering Development Center, June 1979.
2. Heltsley, F. L. and Cline, V. A. "Wing/Store Flow-Field Measurement at Transonic Speeds Using a Laser Velocimeter." AEDC-TR-79-5 (AD-A068328), April 1979.
3. Crosswy, F. L. "Nonorthogonal Measurement Axes in Laser Doppler Velocimetry." AEDC-TR-79-35 (AD-A073700), August 1979.
4. Korn, G. A. and Korn, T. M. *Mathematical Handbook for Scientists and Engineers*. McGraw-Hill, New York, 1961.
5. Jackson, F. M. and Sloan, E. H. "Calibration of the AEDC-PWT 1-Foot Transonic Tunnel." AEDC-TR-68-4 (AD827912), February 1968.
6. Blose, T. G. and Barnes, R. M. "Launch Transient Analysis Essential Element of an Air Launched Weapon Configuration Development." Aircraft/Stores Compatibility Symposium Proceedings, Vol. 1, Arlington, VA, September 1975.
7. Korn, S. C. "Use of the Flow Angularity Technique for Predicting Store Separation Trajectories." Proceedings of the Aircraft/Store Compatibility Symposium, AFFDL-TR-72-67, Vol. 2, August 1972.

8. Hsieh, T. "Analysis of Velocity Measurements about a Hemisphere-Cylinder Using a Laser Velocimeter," *Journal of Spacecraft and Rockets*, Vol. 14, No. 5, May 1977.
9. Farmer, W. M. and Hornkohl, J. O. "Two-Component, Self-Aligning Laser Vector Velocimeter." *Applied Optics*, Vol. 12, No. 11, November 1973, pp. 2636-2640.
10. Crosswy, F. L. and Hornkohl, J. O. "Signal Conditioning Electronics for a Laser Vector Velocimeter." *Review of Scientific Instruments*, Vol. 44, No. 9, September 1973, pp. 1324-1332.
11. Kalb, H. T., Brayton, D. B., and McClure, J. A. "Laser Velocimetry Data Processing." AEDC-TR-73-116 (AD766418), September 1973.
12. Abernethy, R. B., Colbert, D. L., and Powell, B. D. "ICRPG Handbook for Estimating the Uncertainty in Measurements Made With Liquid Propellant Rocket Engine Systems." CPIA No. 180, April 1969.
13. Abernethy, R. B. et al. (Pratt and Whitney Aircraft) and Thompson, J. W. et al. (ARO, Inc.). "Handbook — Uncertainty in Gas Turbine Measurements." AEDC-TR-73-5 (AD755356), February 1973.
14. Crosswy, F. L. and Brayton, D. B. "Design and Evaluation of a Laser Doppler Velocimeter for the AEDC-PWT 4-ft Transonic Tunnel." AEDC-TR-78-30 (AD-A057327), July 1978.

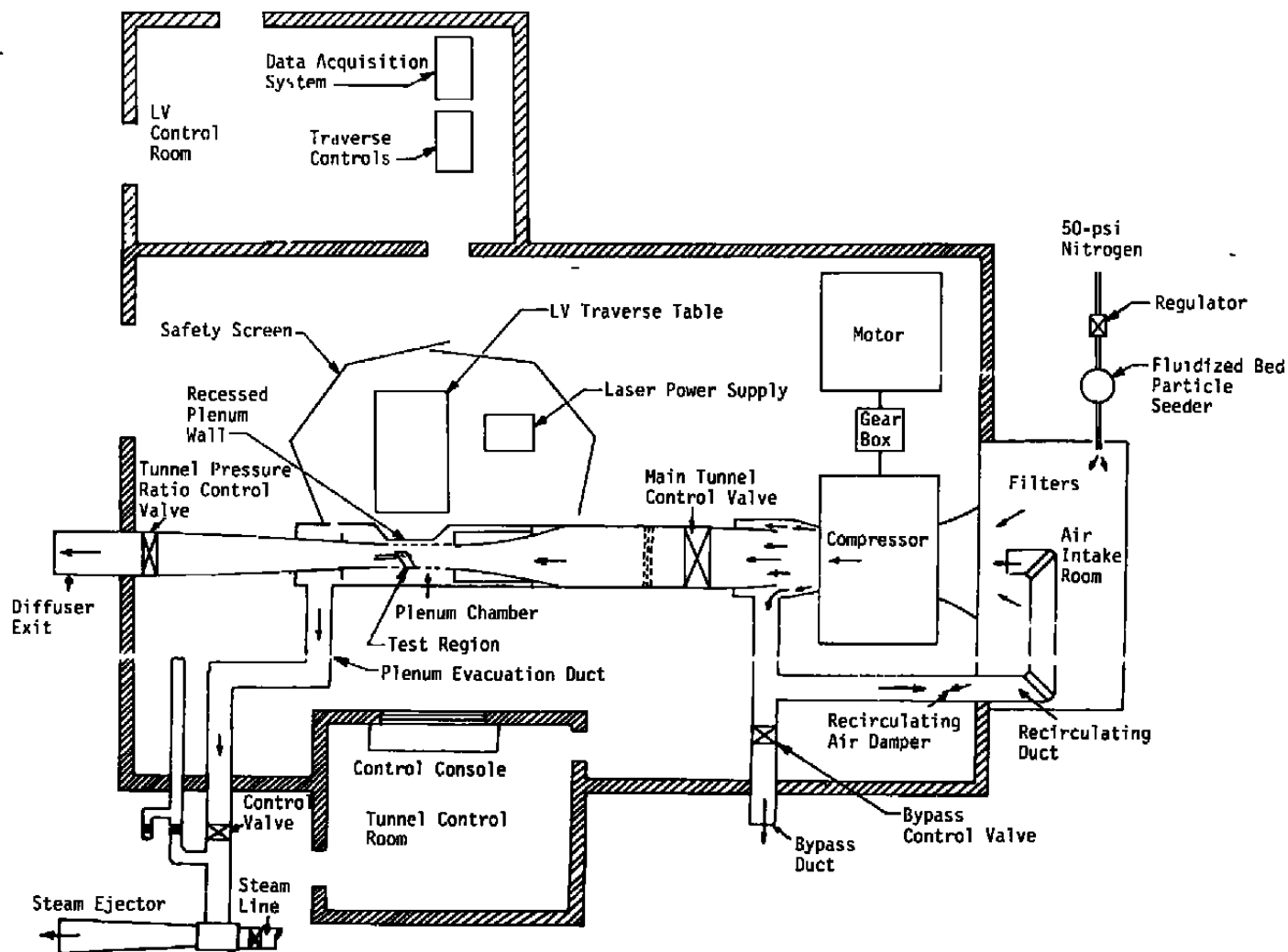
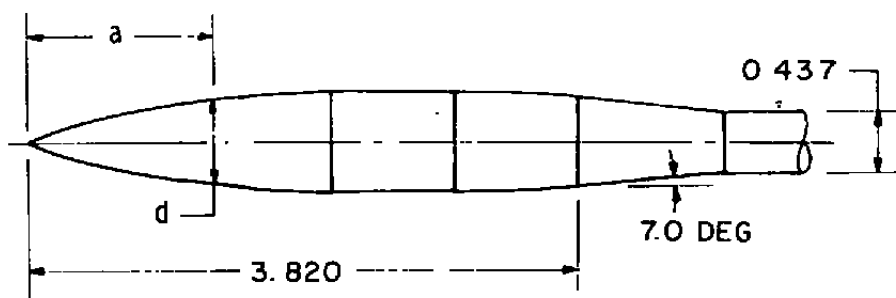
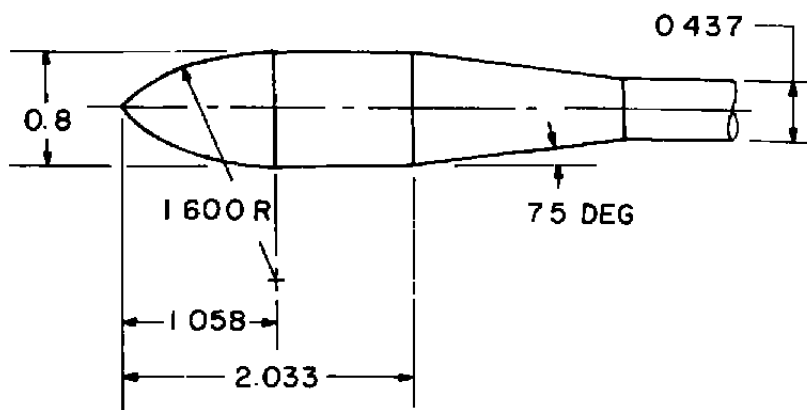


Figure 1. Tunnel 1T layout and LV system installation.



$a$	$d$	$a$	$d$	$a$	$d$
0.0000	0.0000	1.1834	0.5835	2.9833	0.7000
0.2666	0.2313	1.3167	0.6093	3.1166	0.6983
0.3834	0.3073	1.4500	0.6326	3.2500	0.6934
0.5167	0.3777	1.5833	0.6534	3.3833	0.6855
0.6500	0.4349	1.7166	0.6715	3.5166	0.6745
0.7834	0.4819	1.8500	0.6862	3.6500	0.6608
0.9167	0.5211	1.9833	0.6961	3.7833	0.6403
1.0500	0.5545	2.1166	0.7000	3.8200	0.6392

a. MK-83

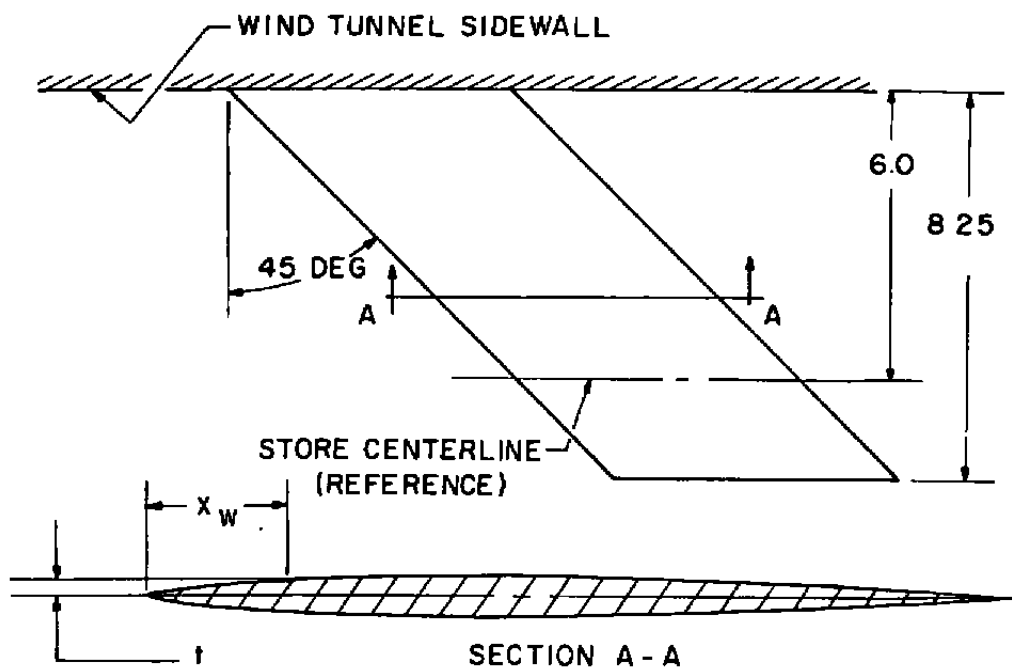


ALL DIMENSIONS IN INCHES

b. M-117

Figure 2. Model dimensions.





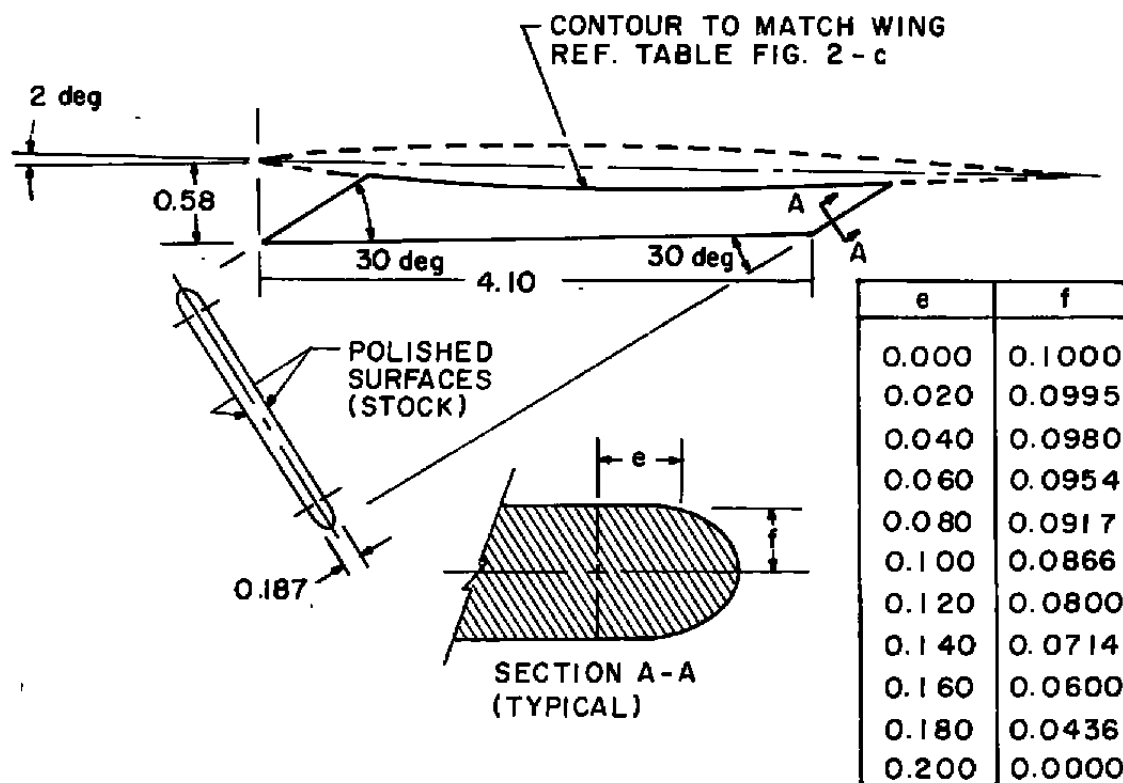
$x_w$	$t$
0.0000	0.0000
0.0065	0.0095
0.0750	0.0284
0.1500	0.0420
0.3000	0.0623
0.4500	0.0783
0.6000	0.0914
0.9000	0.1124
1.2000	0.1274

$x_w$	$t$
1.8000	0.1450
2.4000	0.1500
3.0000	0.1456
3.6000	0.1330
4.2000	0.1120
4.8000	0.0830
5.4000	0.0466
5.7000	0.0256
6.0000	0.0000

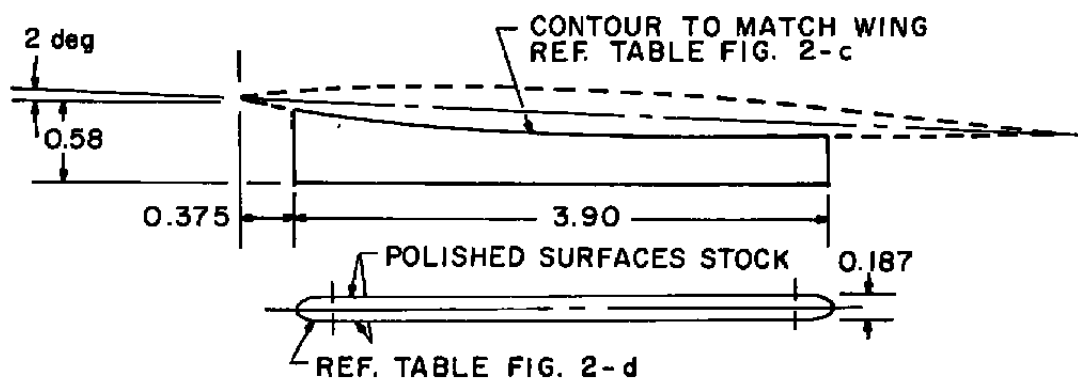
ALL DIMENSIONS IN INCHES

c. Wing

Figure 2. Continued.



d. Swept pylon



e. Unswept pylon

Figure 2. Concluded.

CONFIGURATION

W	P	S
---	---	---

W = 0 NO WING

1 WING AT  $\alpha_w = 0$  deg2 WING AT  $\alpha_w = 2.0$  deg

P = 0 NO PYLON

1 UNSWEPT PYLON

2 SWEPT PYLON

S = 0 NO STORE

1 MK - 83

2 M - 117

Configuration convention of Ref. 2 was modified  
to include pylons and incidence angles.

Figure 3. Configuration identification.

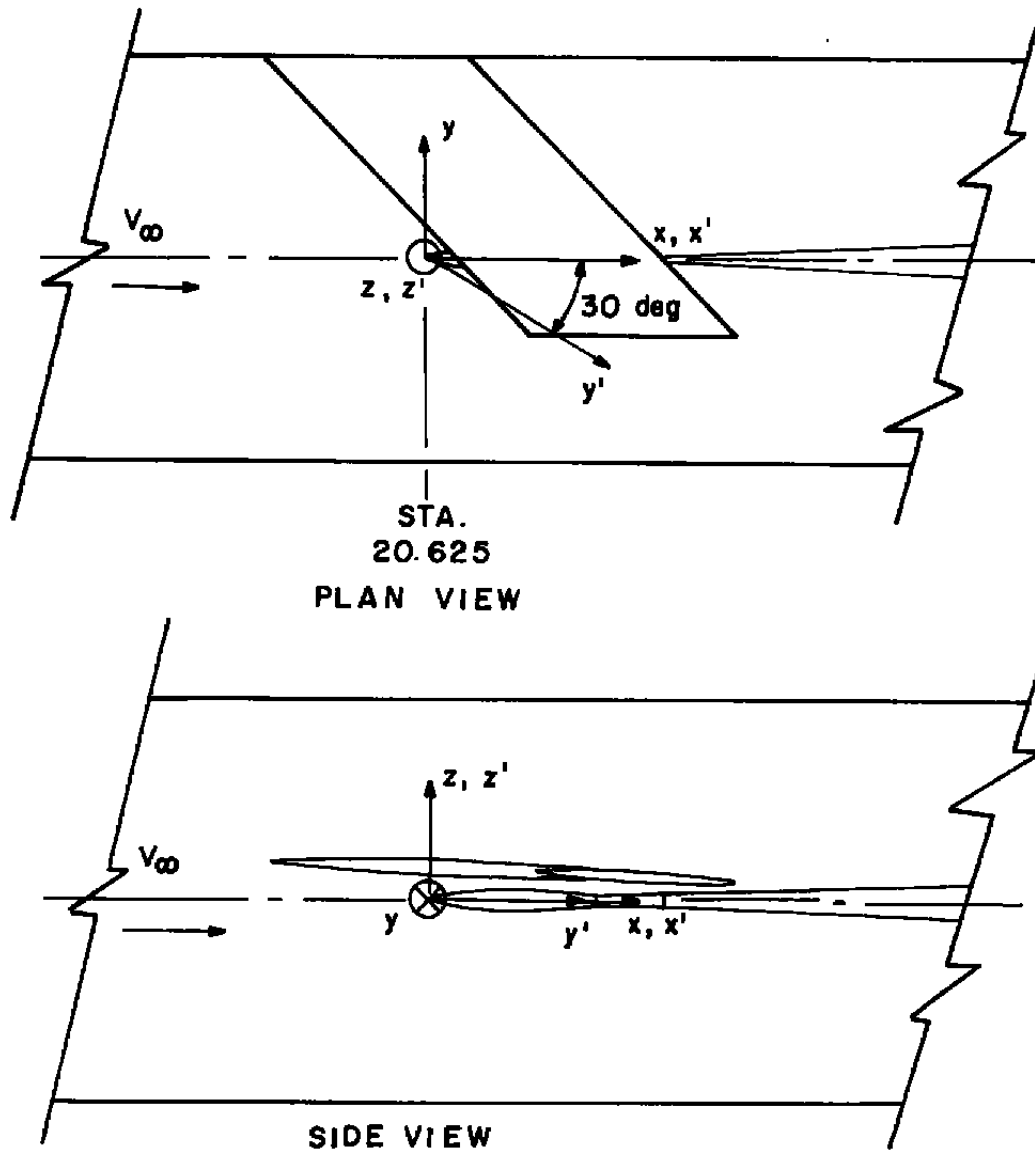
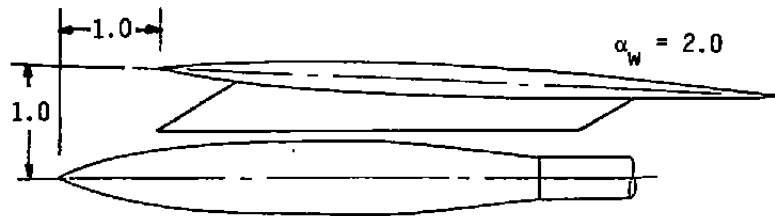
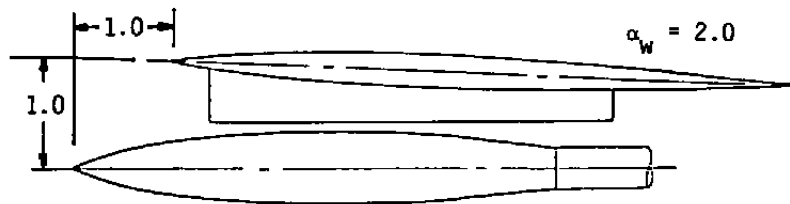


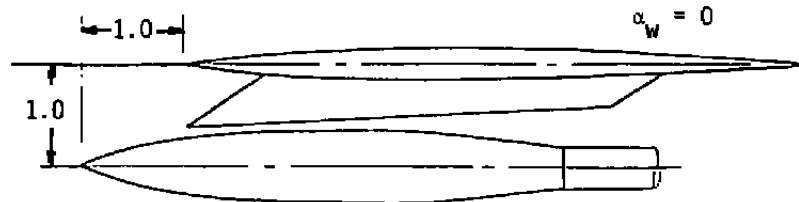
Figure 4. Coordinate system definition.



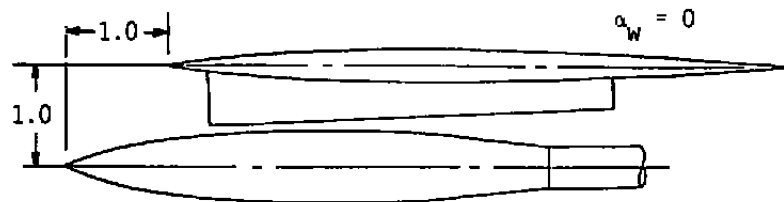
a. Configuration 221



b. Configuration 211



c. Configuration 121



d. Configuration 111



e. Configuration 122

Figure 5. Basic wing/pylon/store configurations.

All Dimensions in Inches

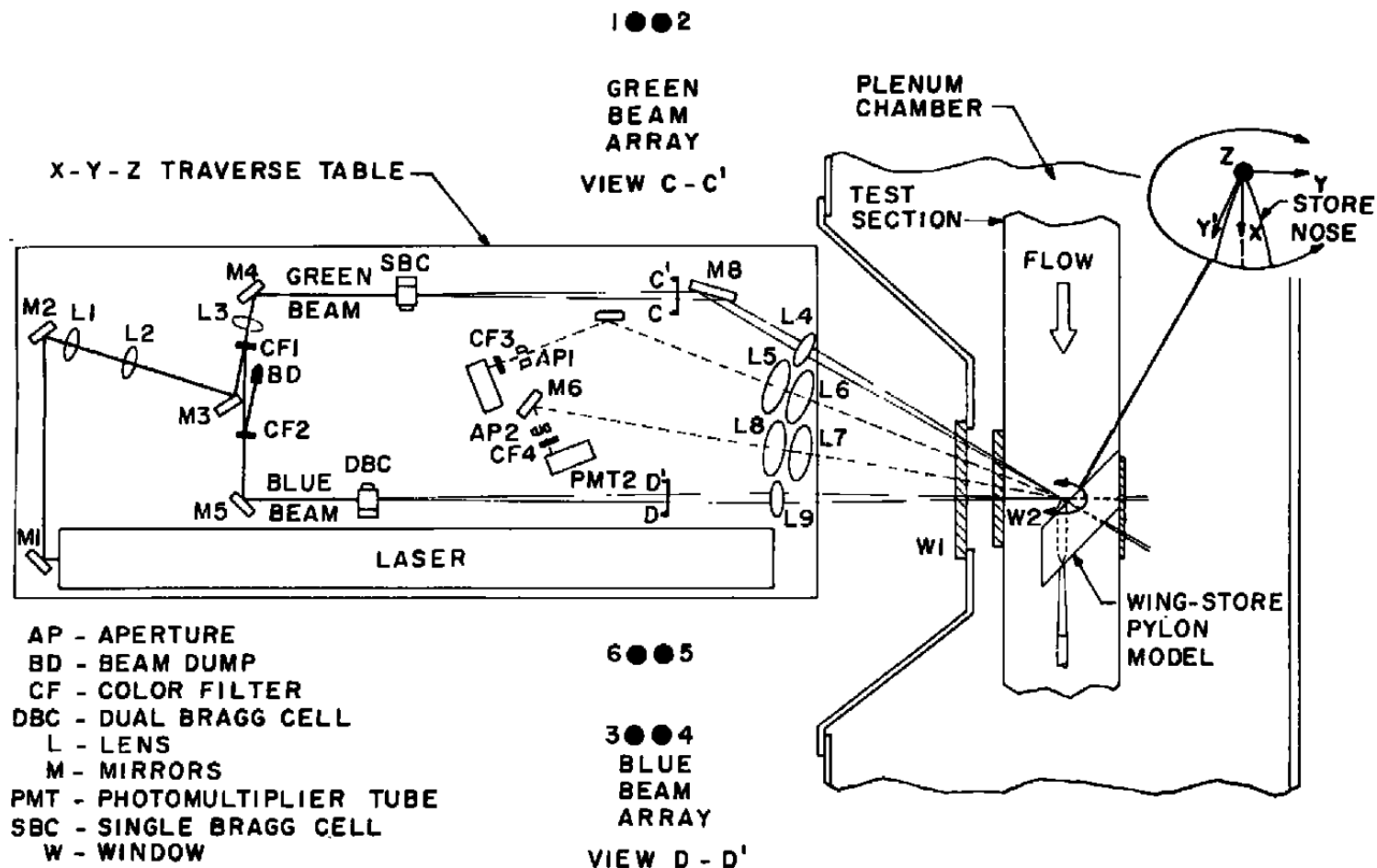


Figure 6. Tunnel 1T three-velocity component LV optical system installation.

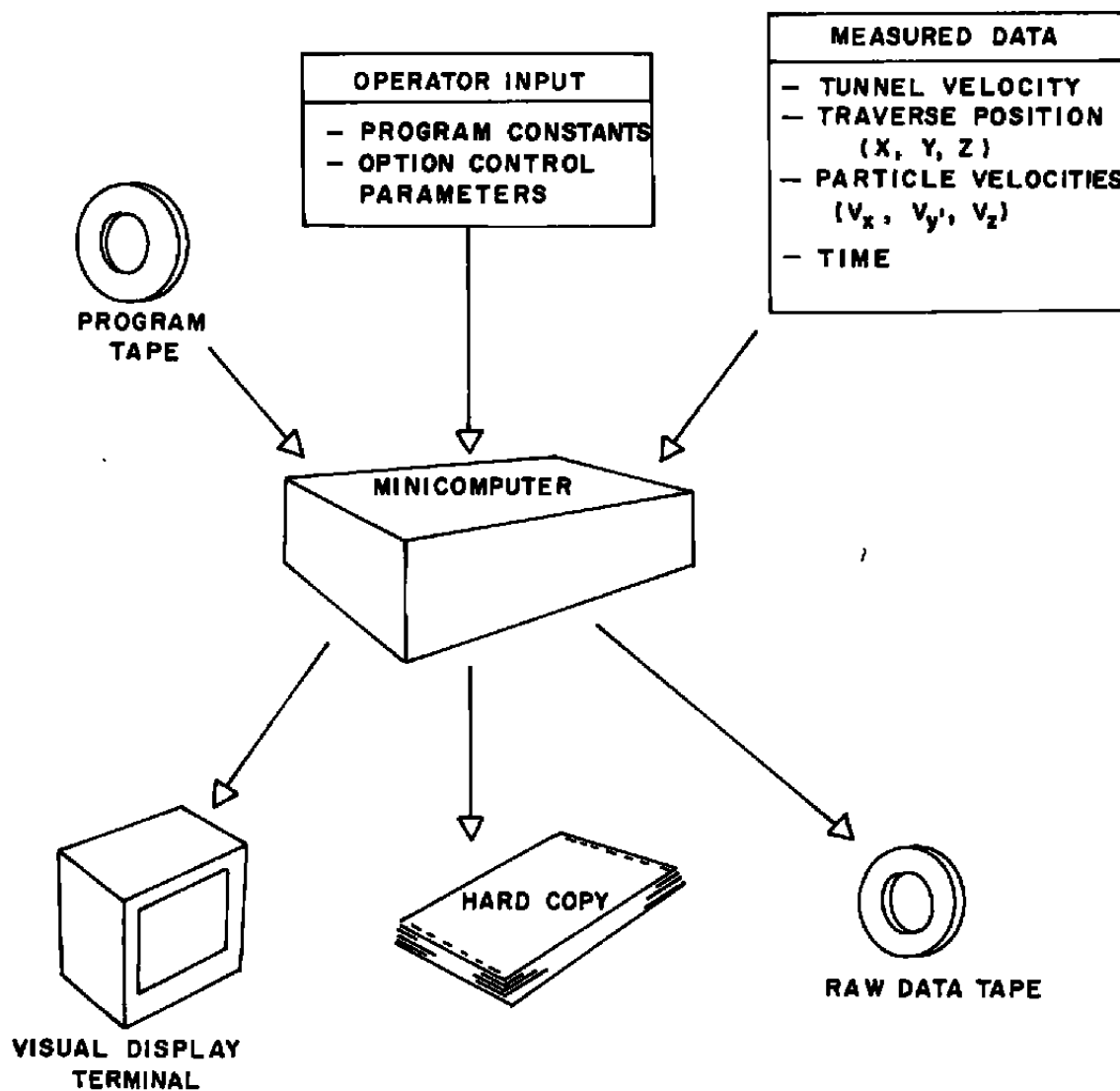


Figure 7. LV data acquisition system schematic.

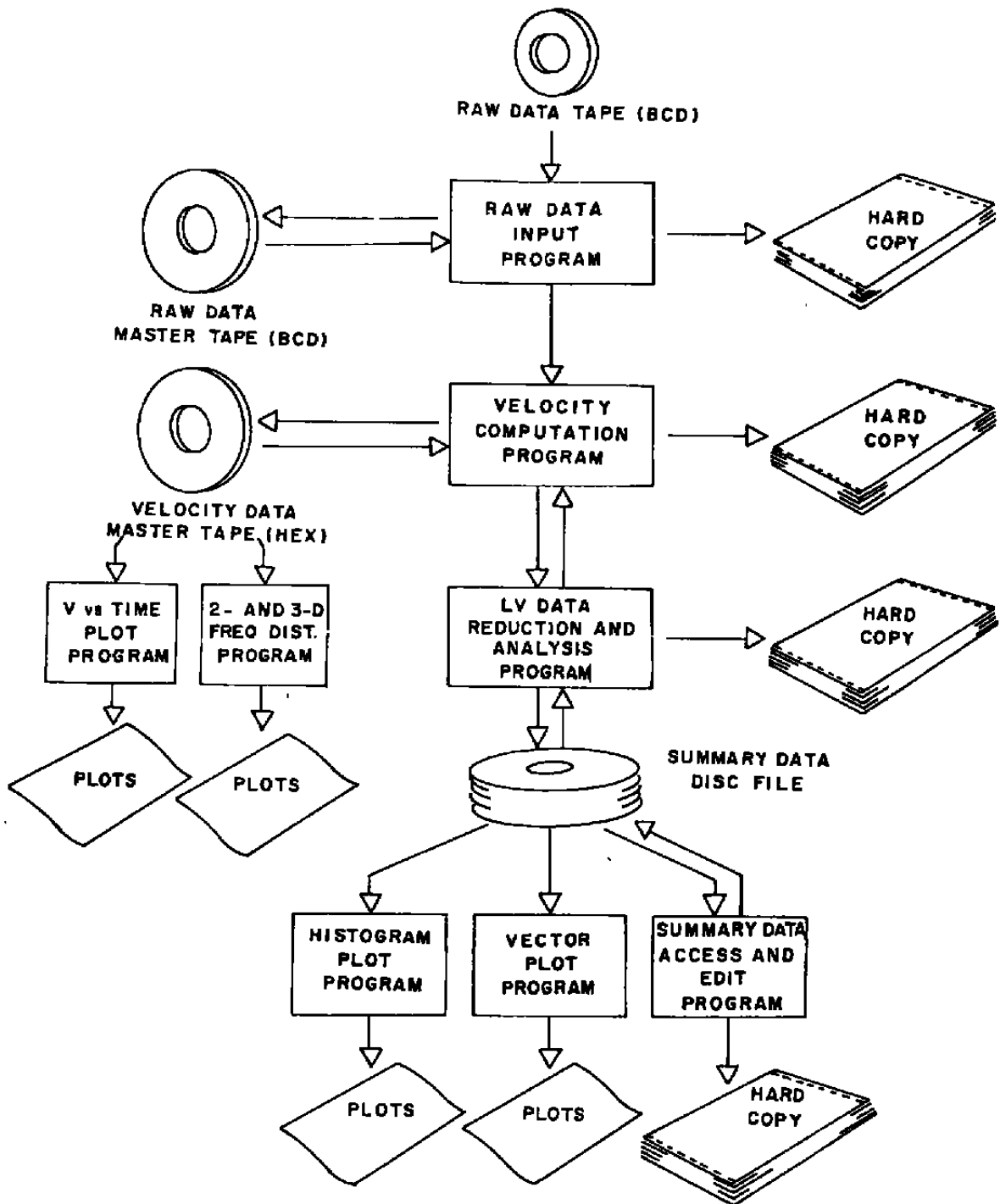


Figure 8. Offline data processing sequence.



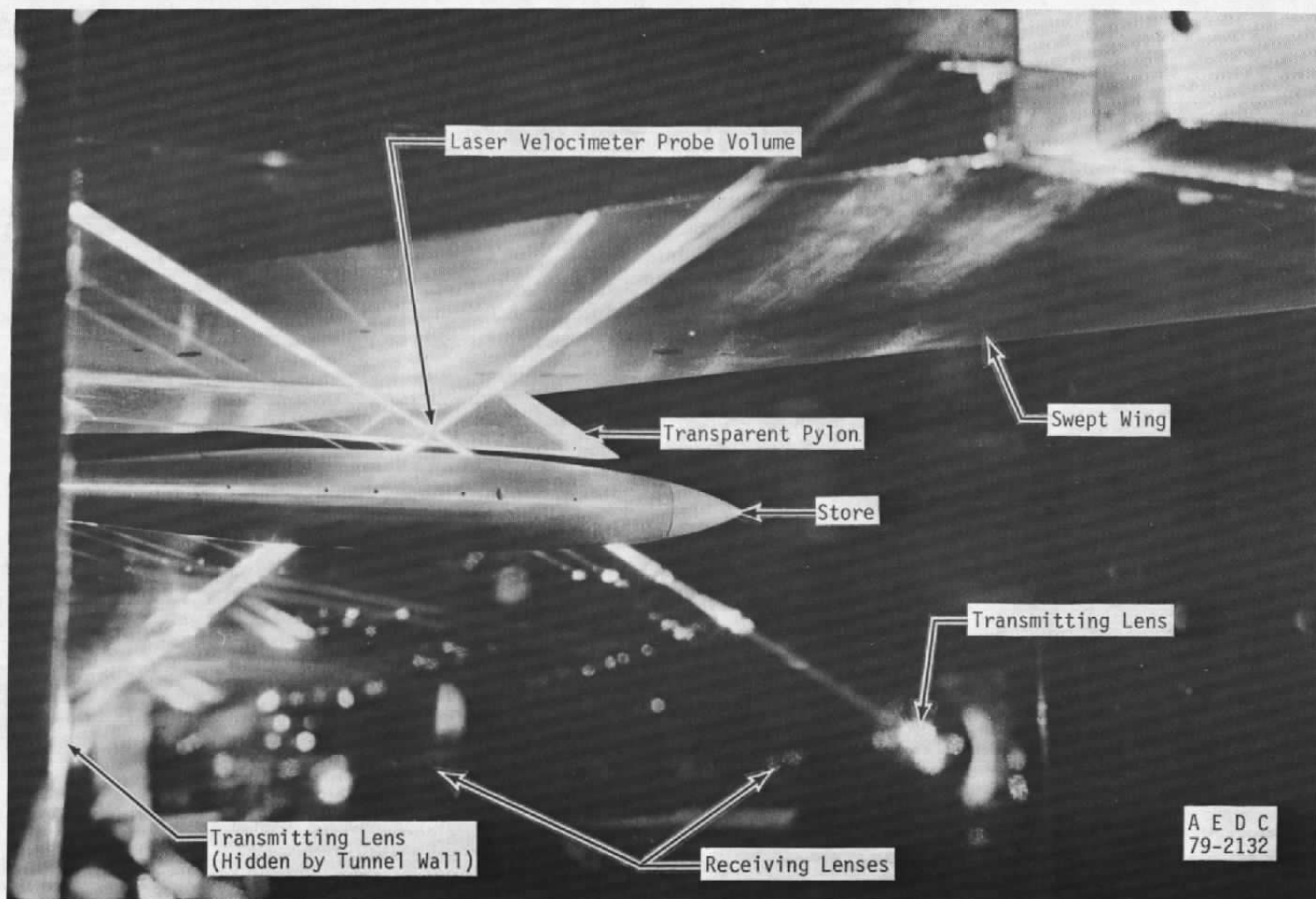
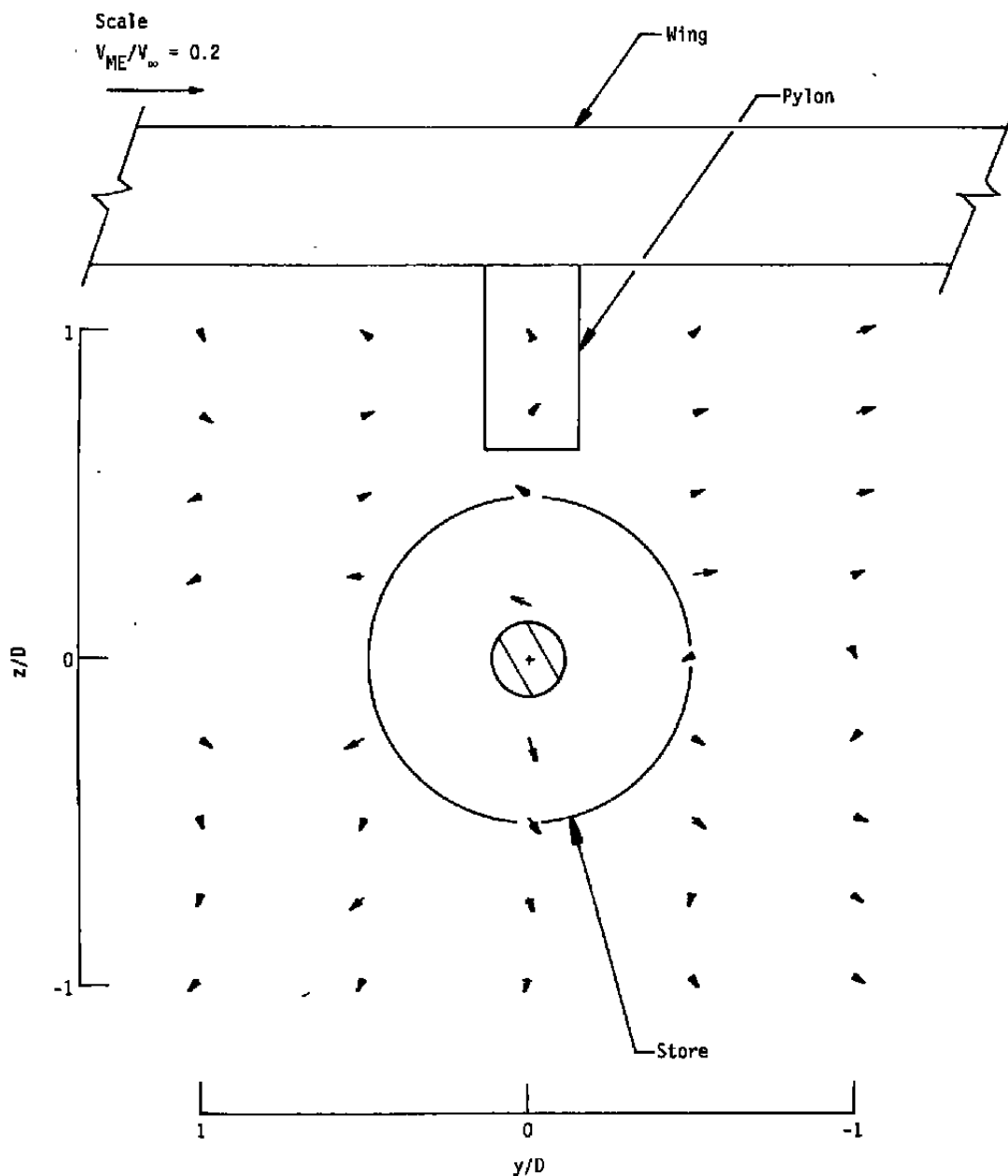


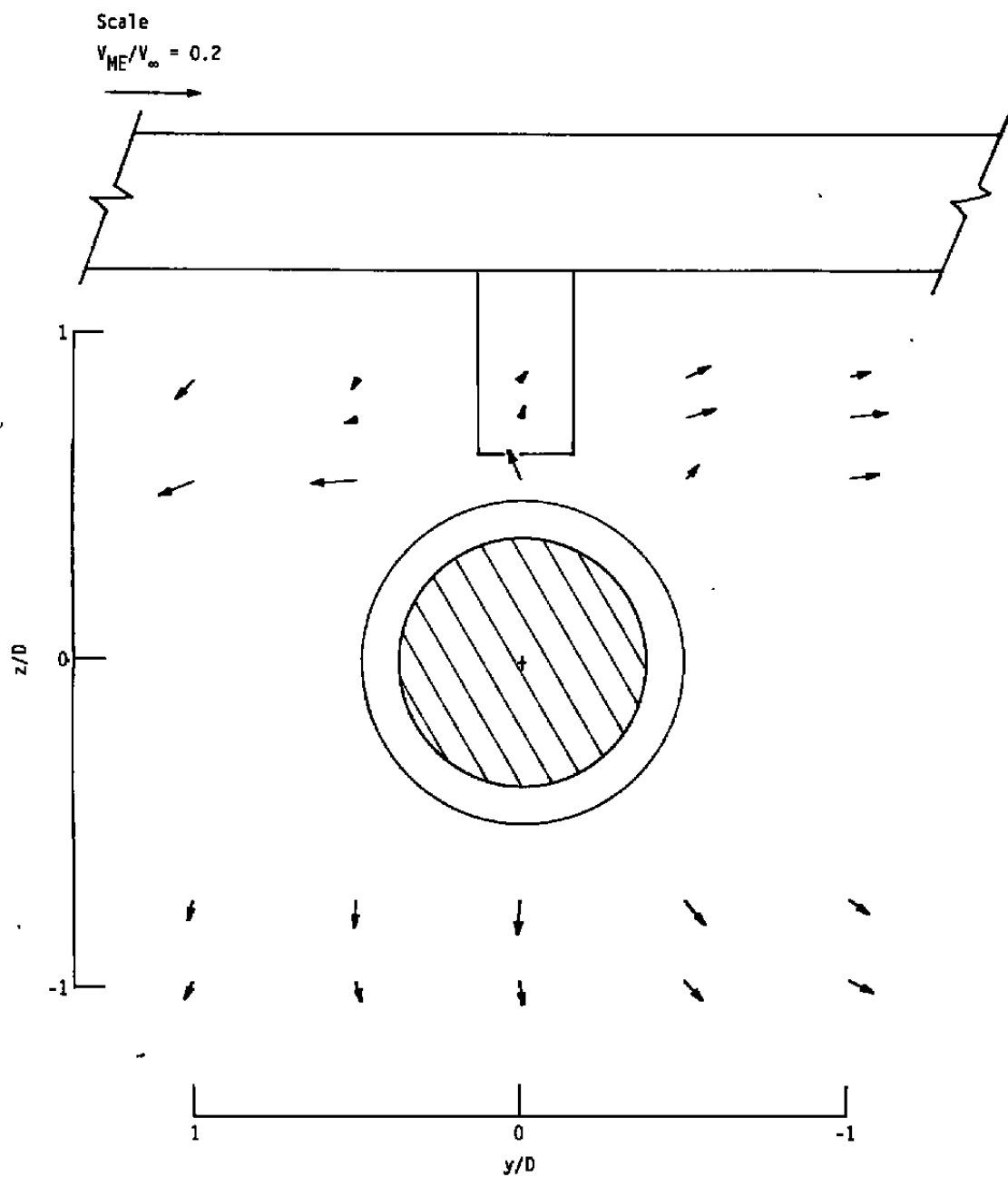
Figure 9. Configuration 221 installed in tunnel 1T with the three-component LV beams passing through the gap between the pylon and store.



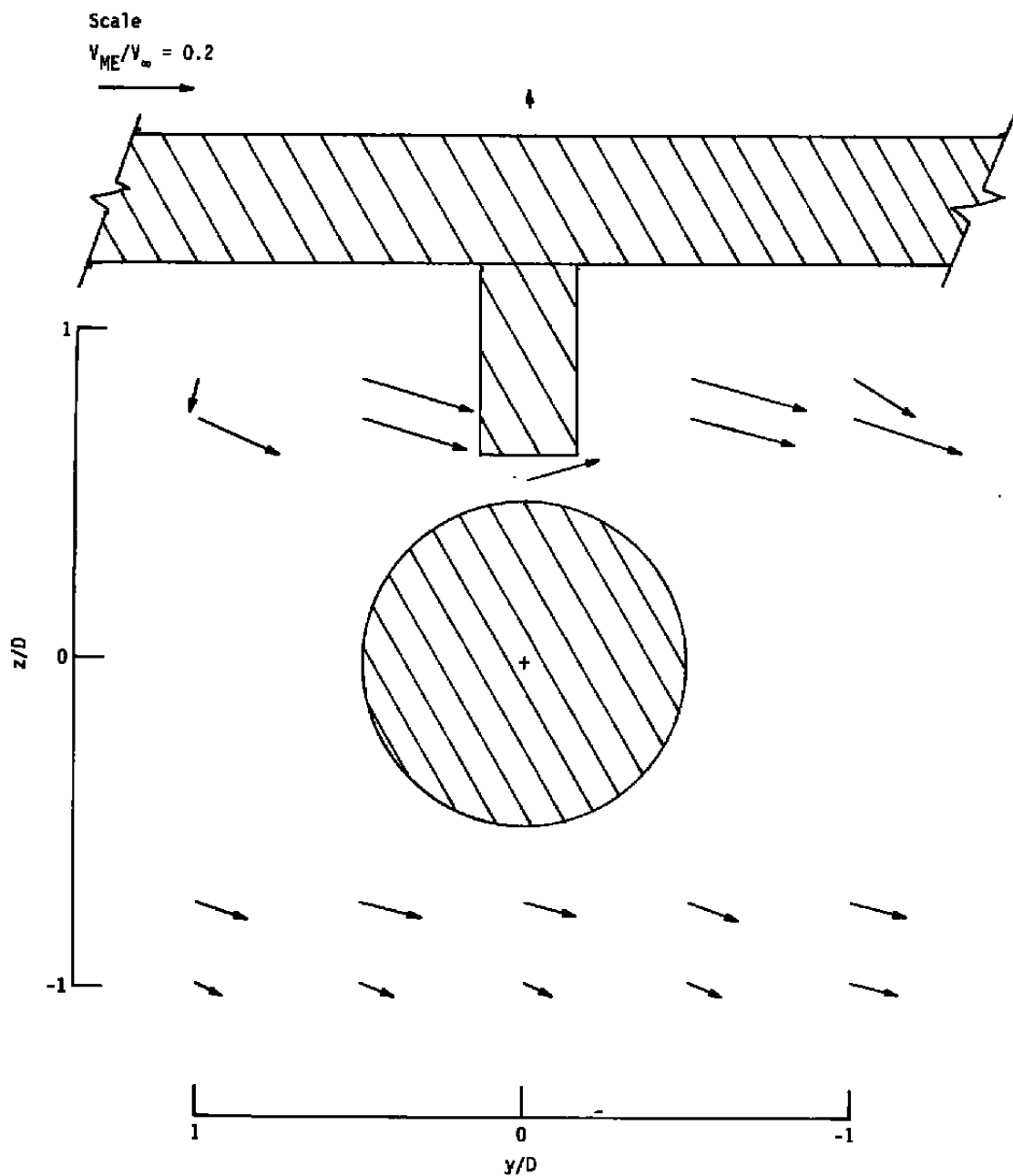
The crosshatched area indicates model cross section at this  $x/D$  station.

a.  $x/D = 0.20$

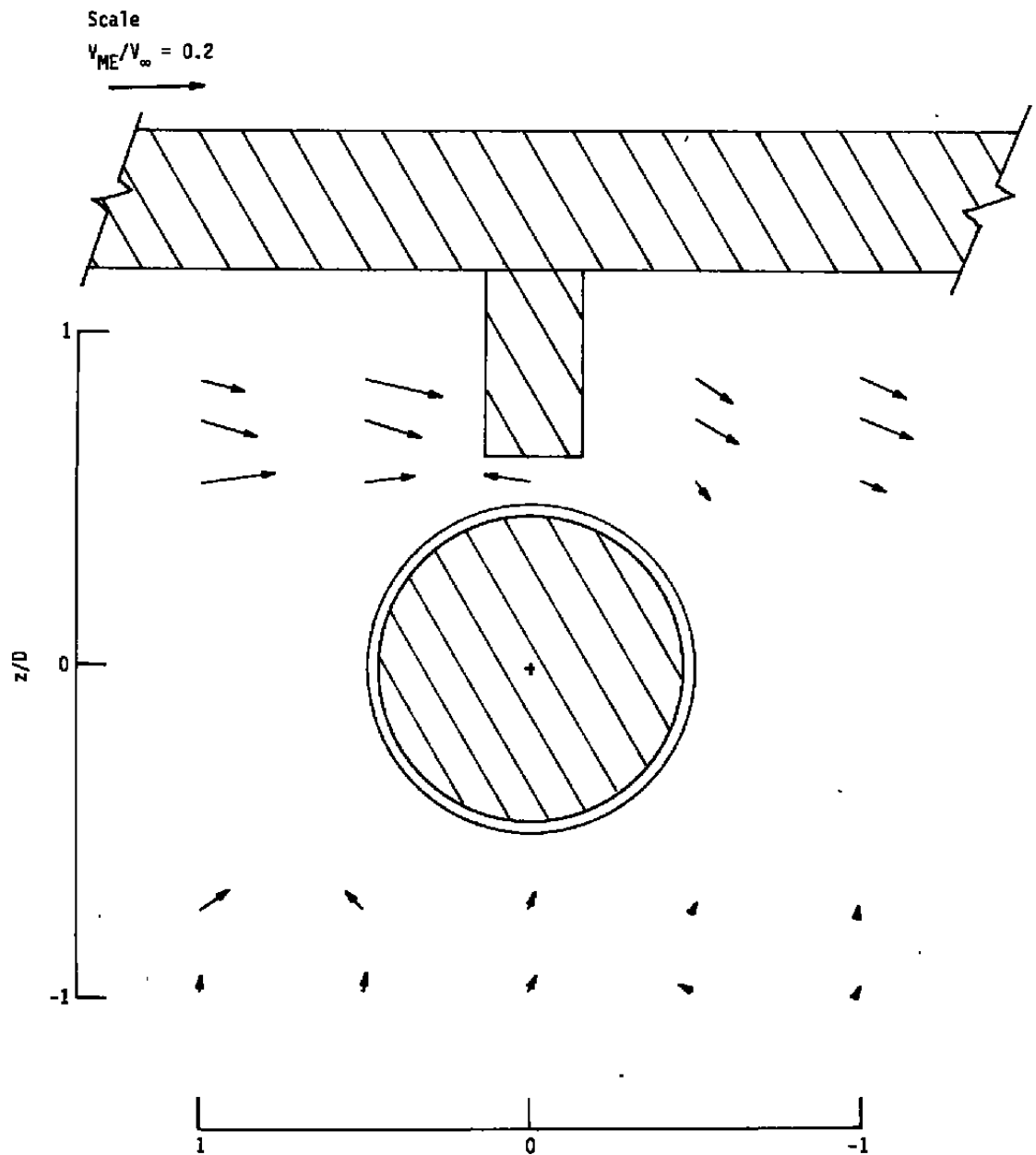
Figure 10. Mean velocity vector projections in constant  $x$  planes for configuration 111 ( $\alpha_w = 0$ ),  $M_{\infty} = 0.92$ .



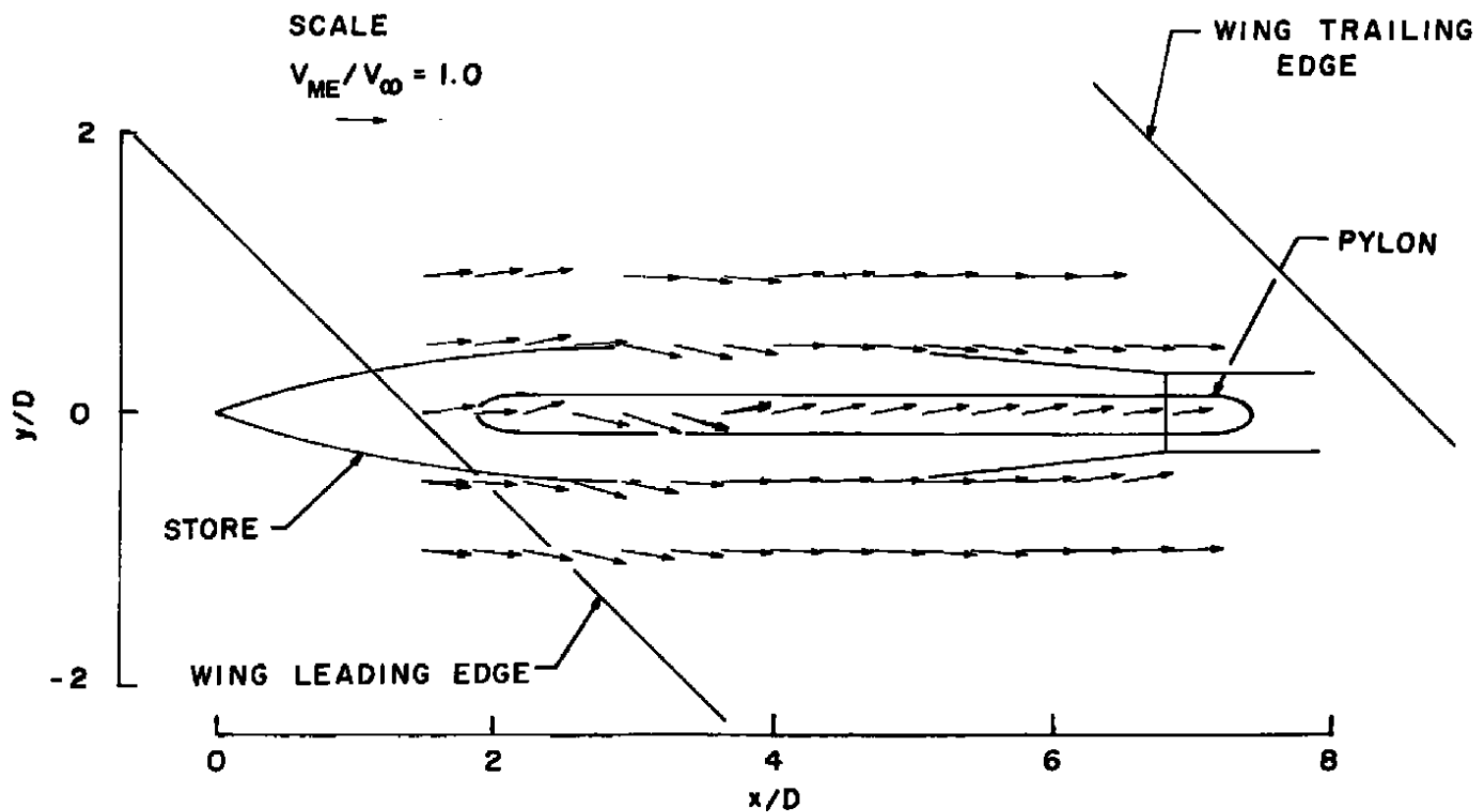
b.  $x/D = 1.43$   
Figure 10. Continued.



c.  $x/D = 3.20$   
 Figure 10. Continued.

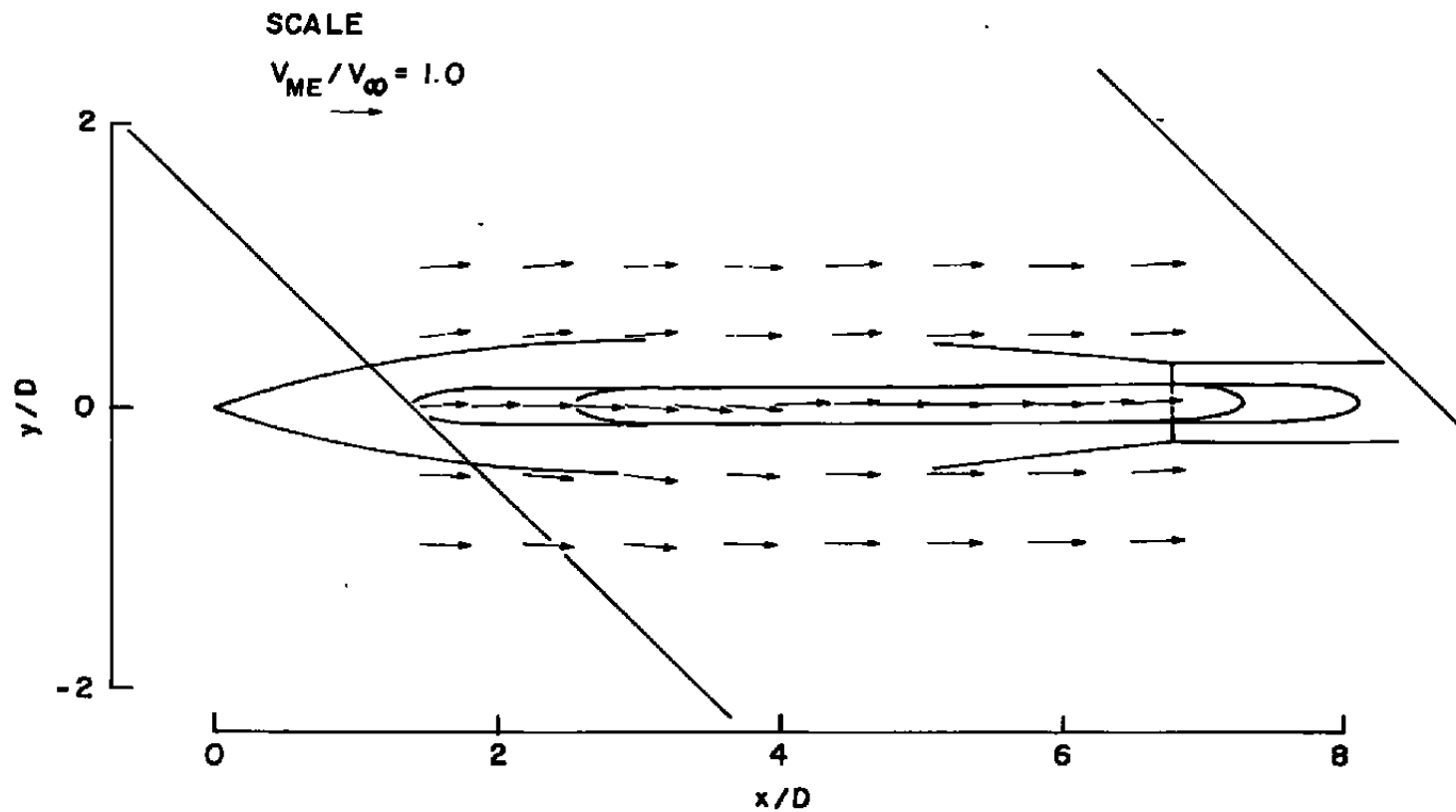


d.  $x/D = 5.7$   
Figure 10. Concluded.

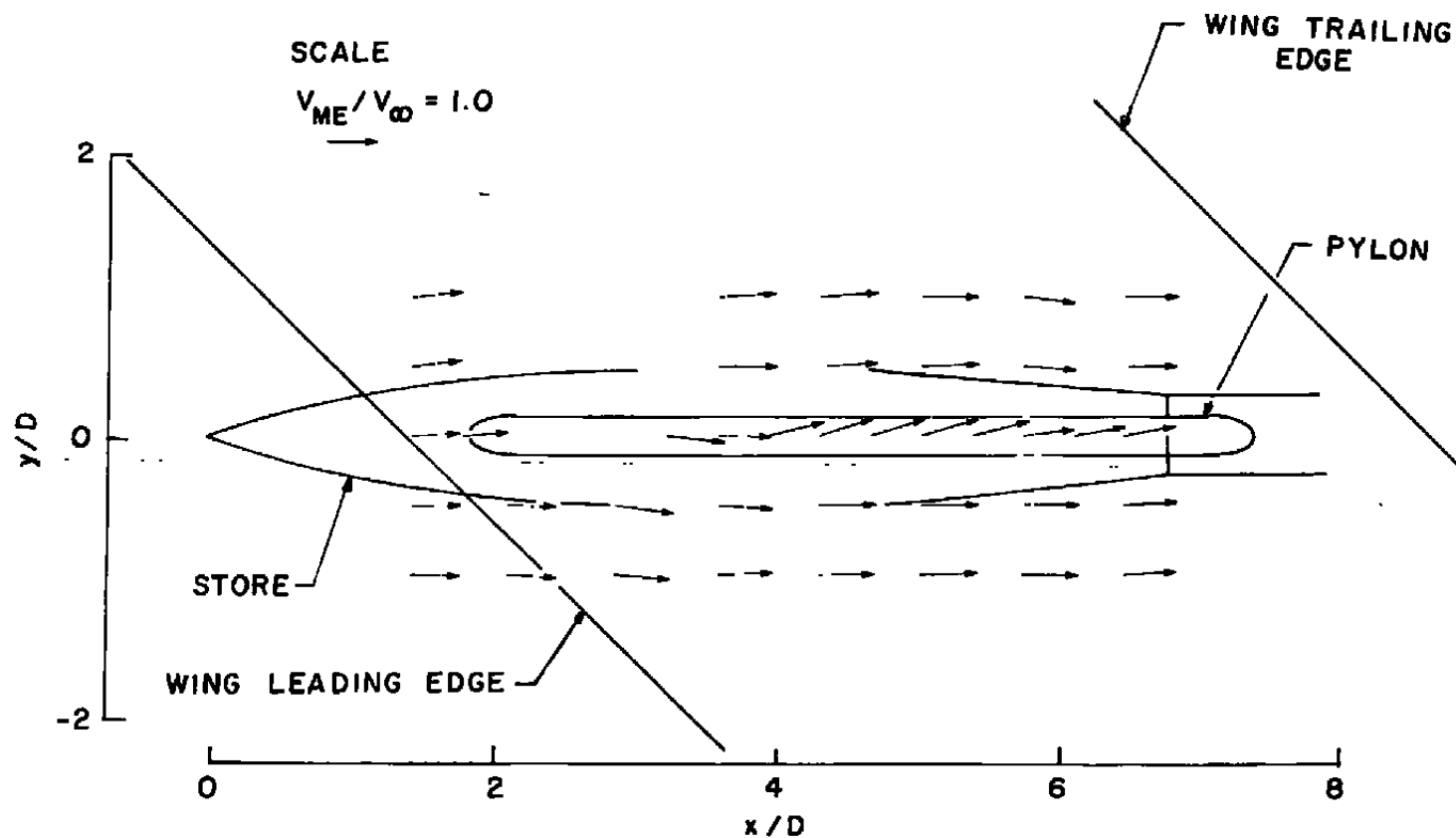


a. Configuration 211

Figure 11. Effect of pylon on mean velocity vector projections in constant  $z$  plane for two wing/MK-83 configurations ( $a_w = 2.0$ ),  $M_{\infty} = 0.92$ ,  $z/D = 0.56$ .



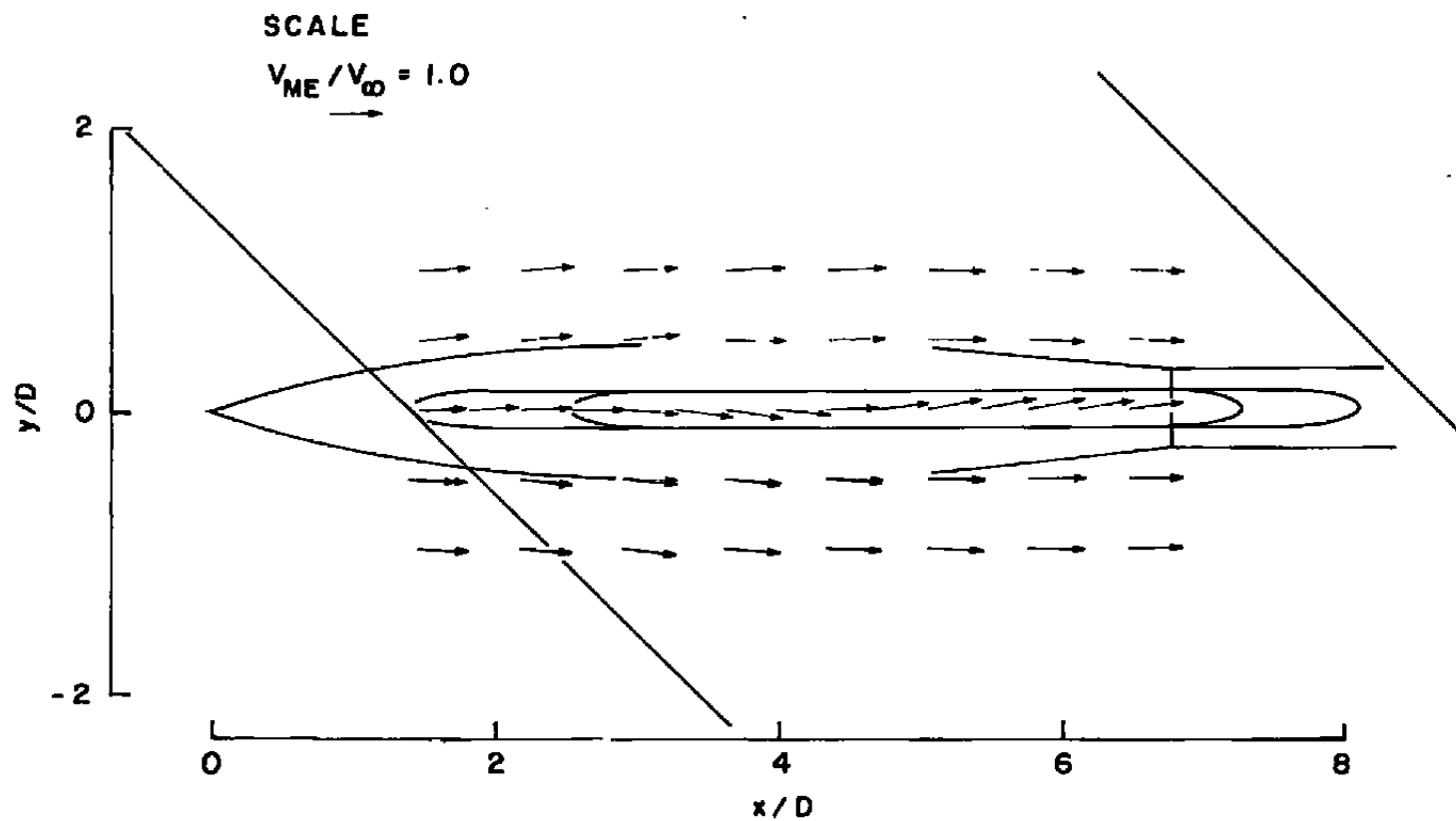
b. Configuration 221  
 Figure 11. Concluded.



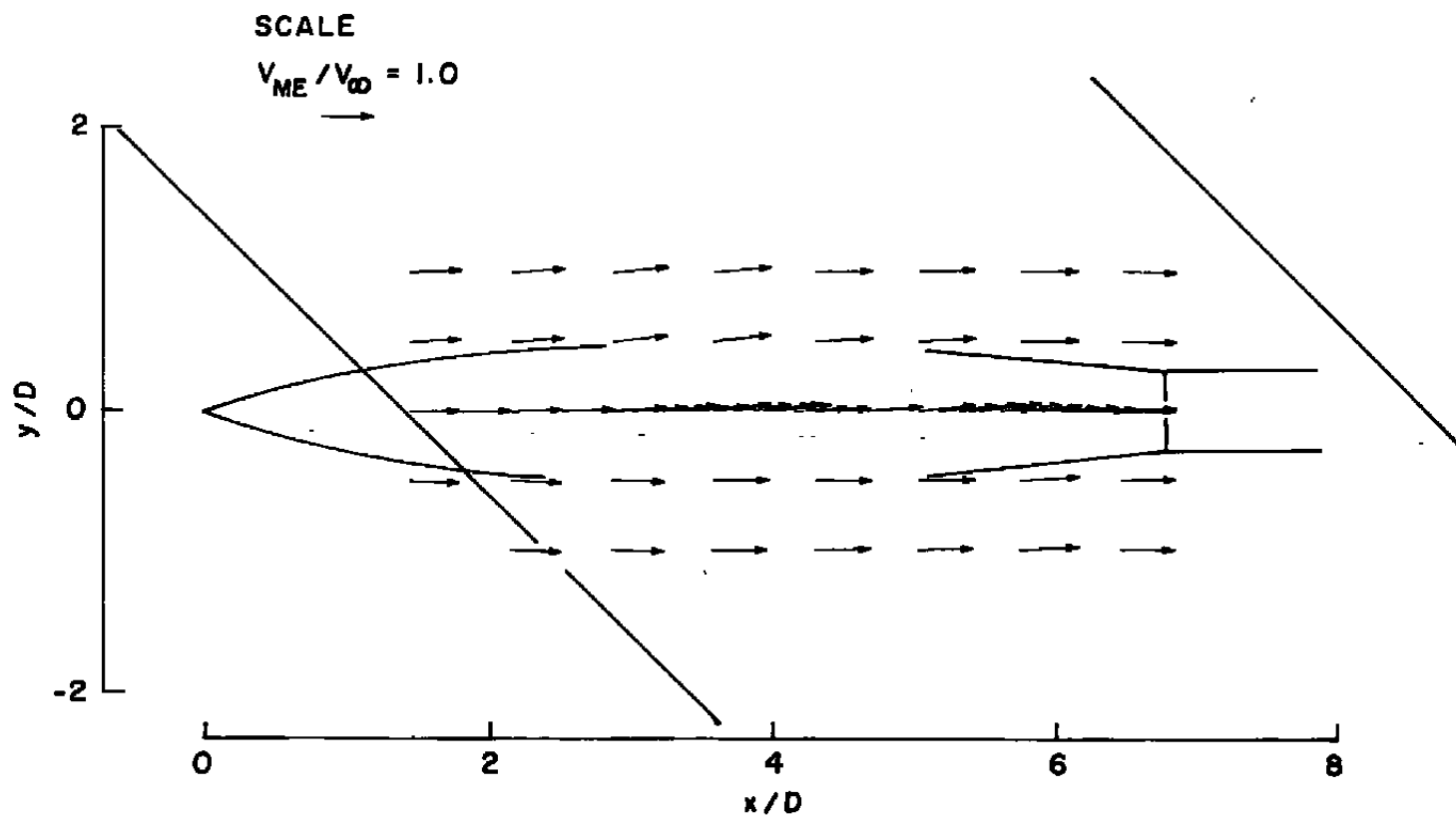
a. Configuration 111

Figure 12. Effects of pylon on velocity vector projections in constant  $z$  plane for four wing/MK-83 configurations ( $\alpha_w = 0$ ),  $M_{\infty} = 0.92$ ,  $z/D = 0.56$ .

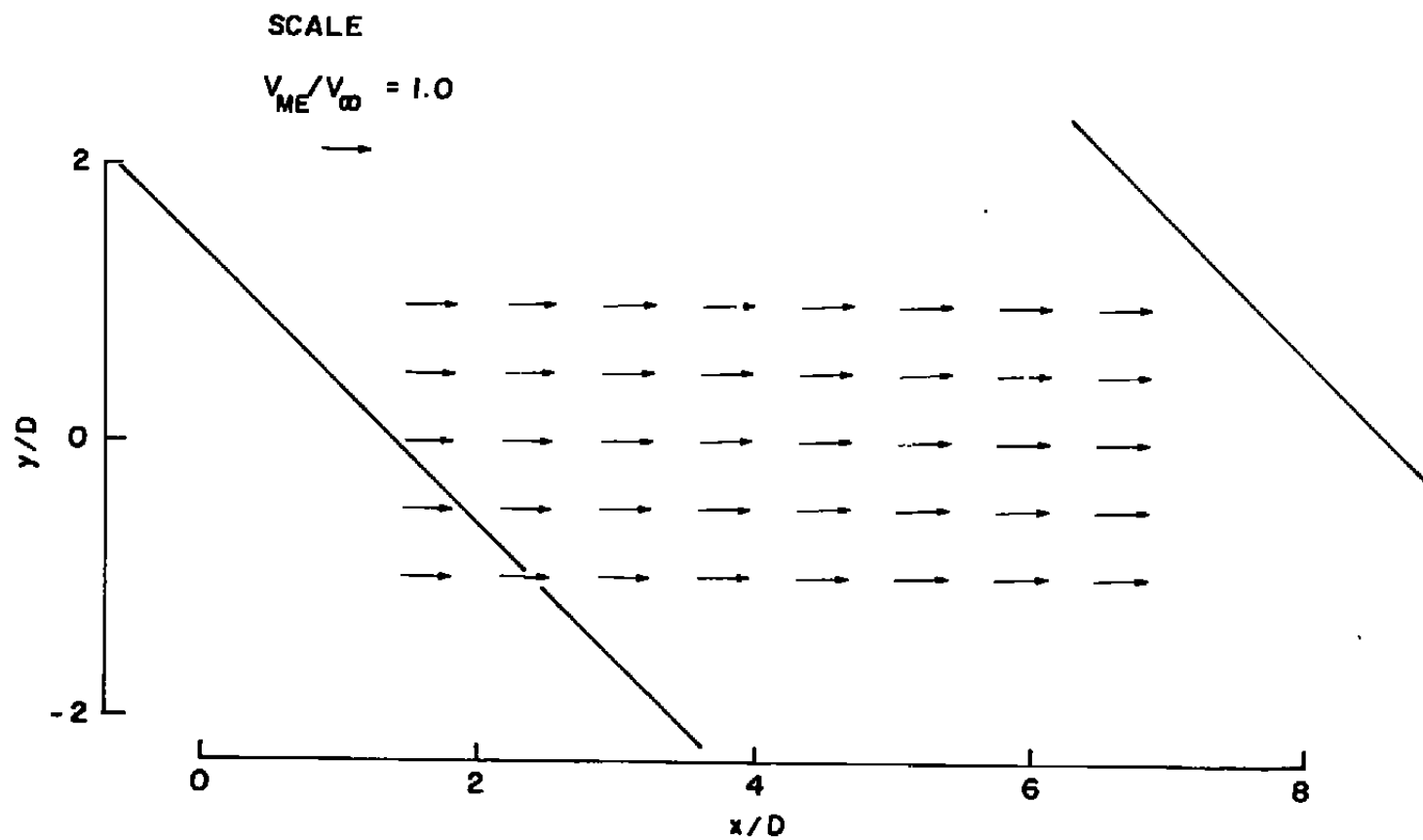




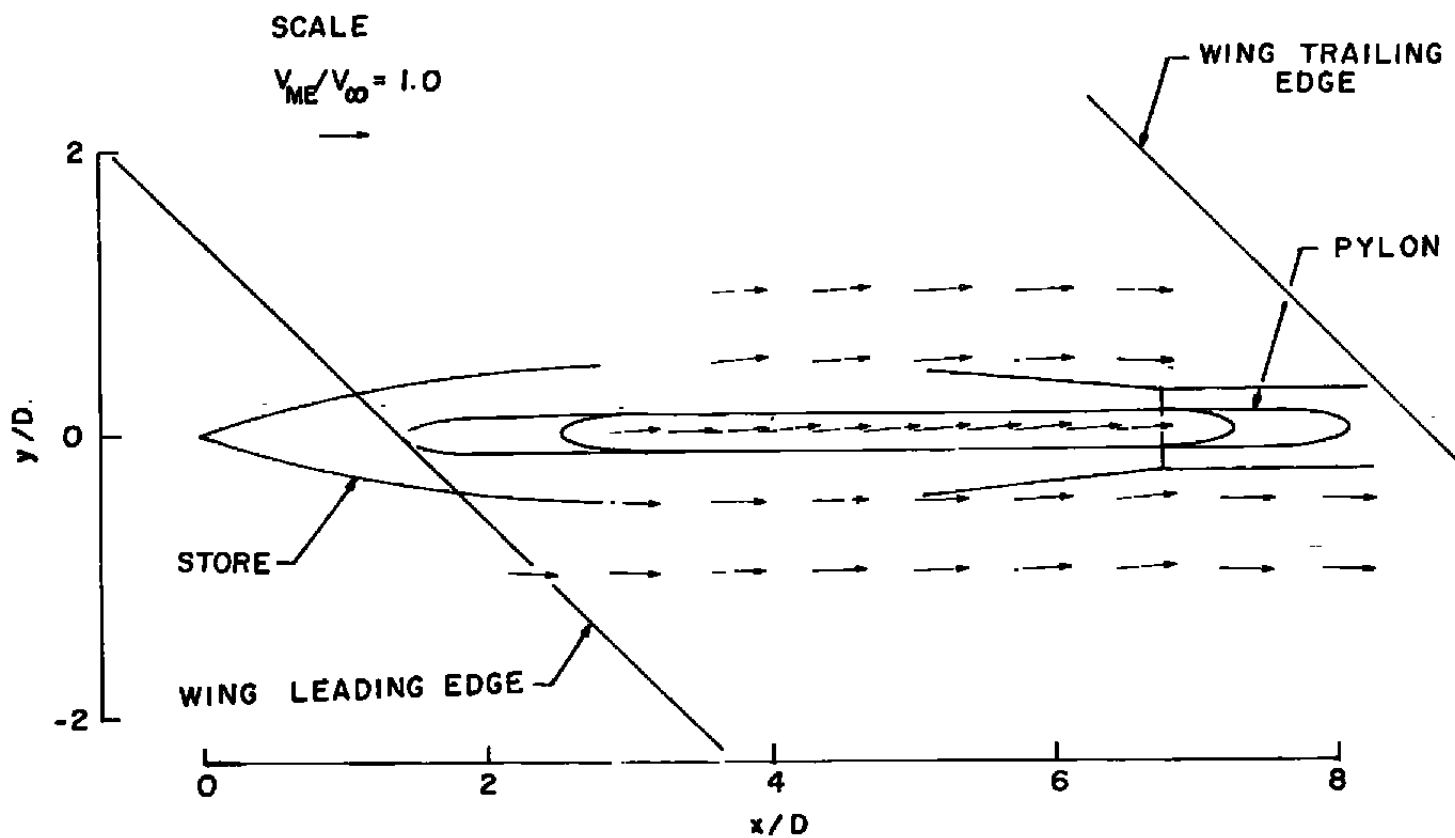
b. Configuration 121  
 Figure 12. Continued.



c. Configuration 101  
Figure 12. Continued.

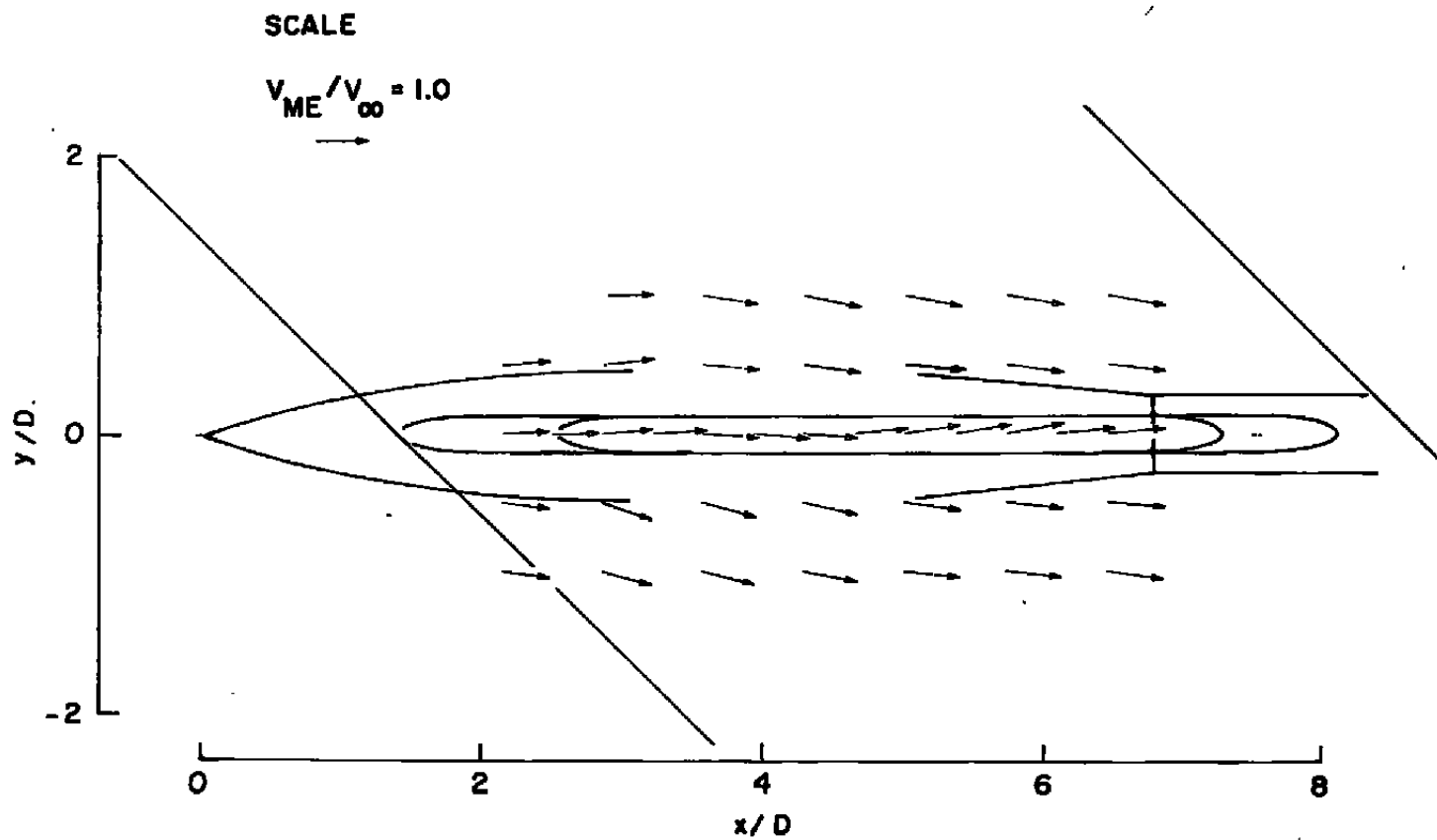


d. Configuration 100  
Figure 12. Concluded.

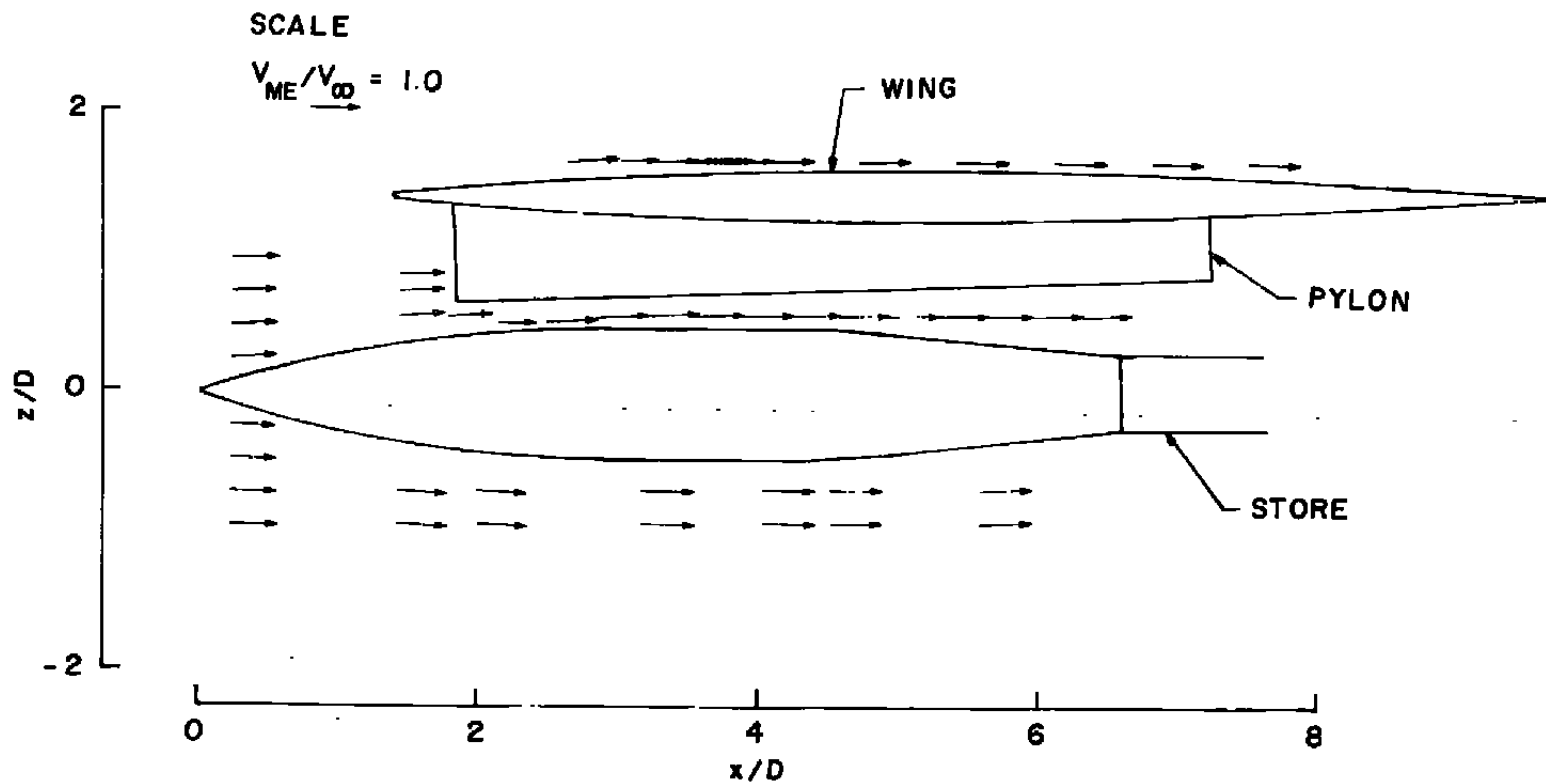


a.  $M = 0.975$

Figure 13. Effect of Mach number on mean velocity vector projections in constant  $z$  plane for three wing/MK-83 configurations ( $\alpha_w = 0$ ),  $M_{\infty} = 0.92$ ,  $y/D = 0$ .

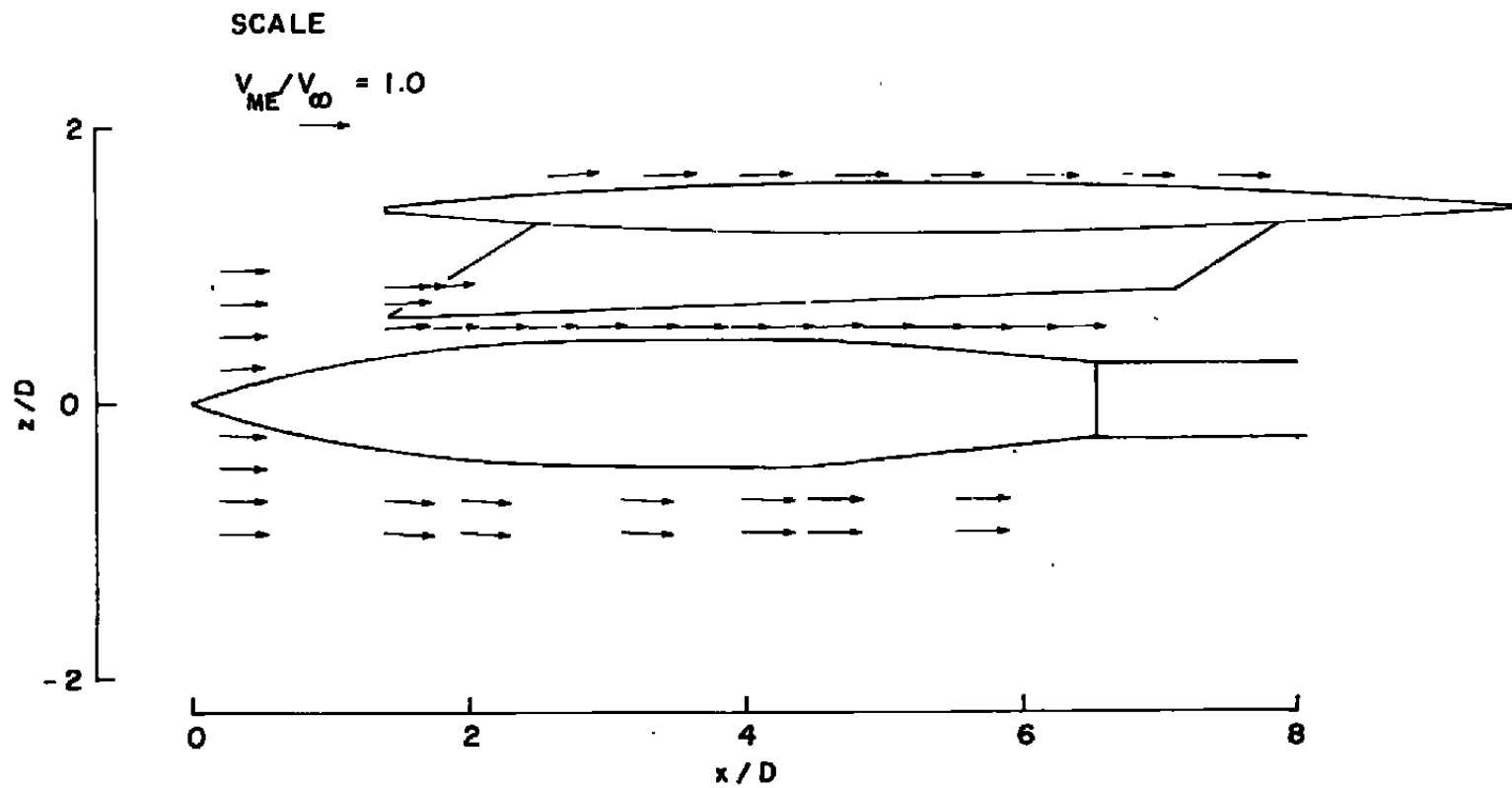


b.  $M_{\infty} = 1.025$   
Figure 13. Concluded.

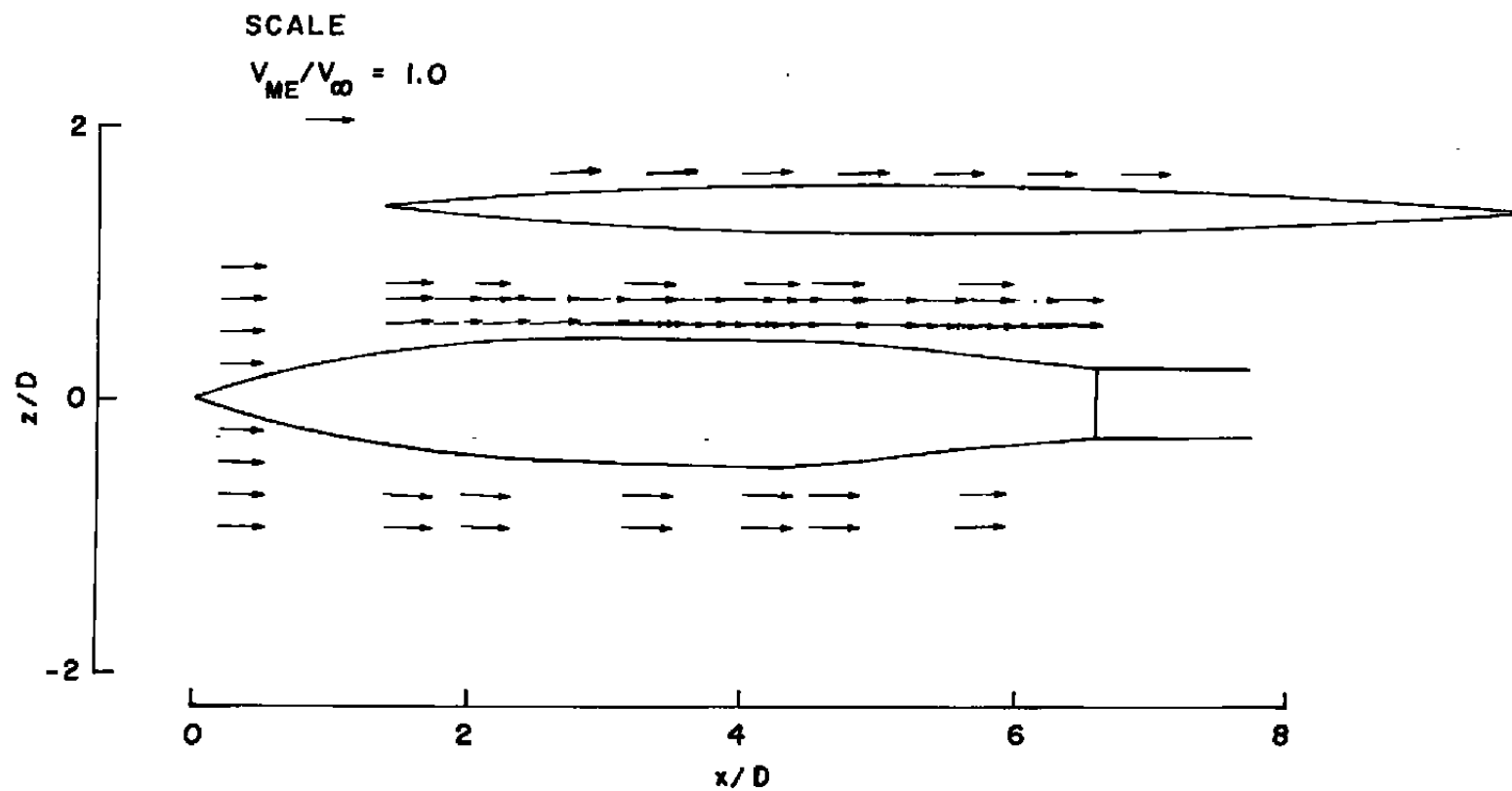


a. Configuration 111

Figure 14. Effect of pylon on velocity vector projections in constant y plane for three wing/MK-83 configurations ( $\alpha_w = 0$ ),  $M_{\infty} = 0.92$ ,  $y/D = 0$ .

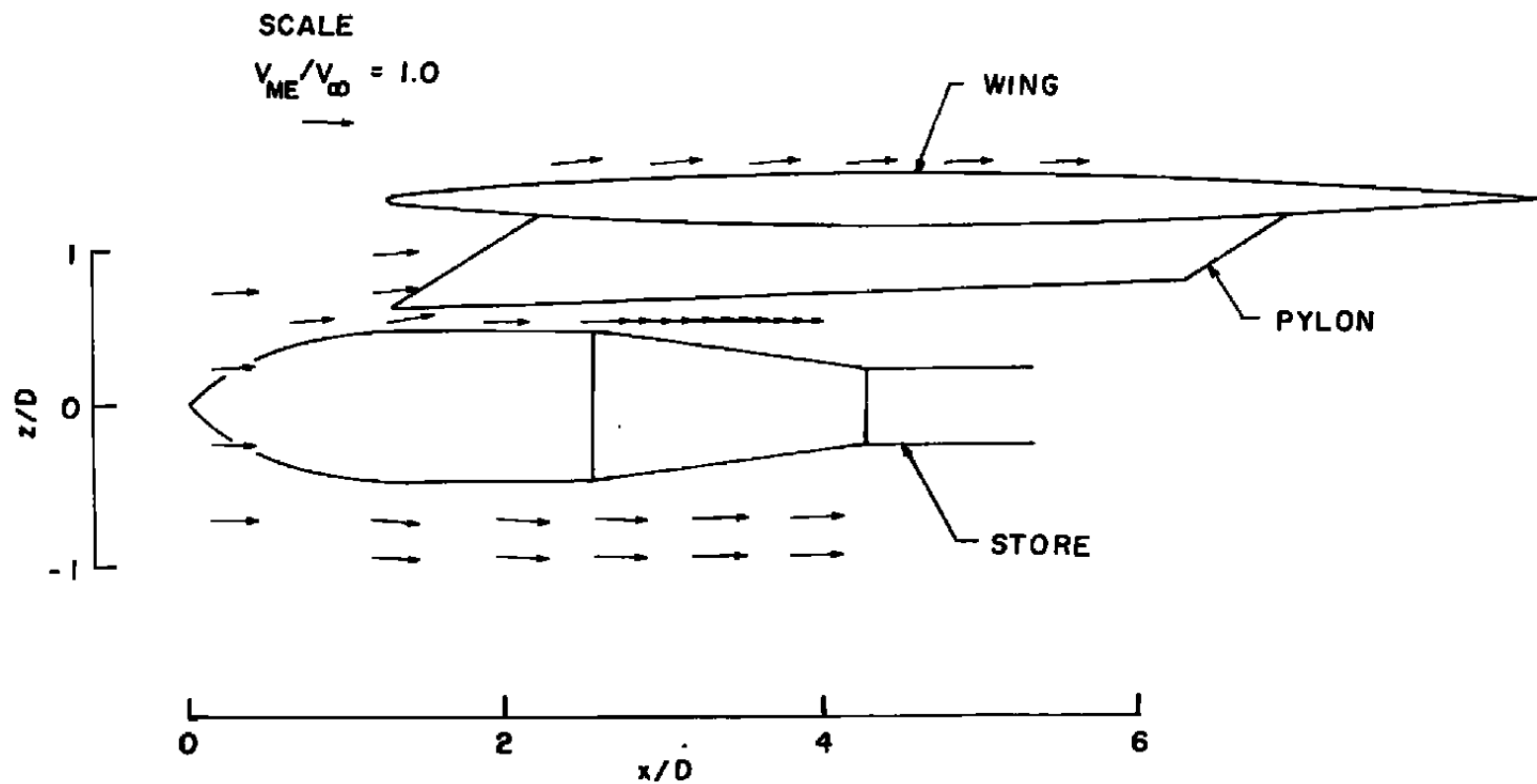


b. Configuration 121  
Figure 14. Continued.



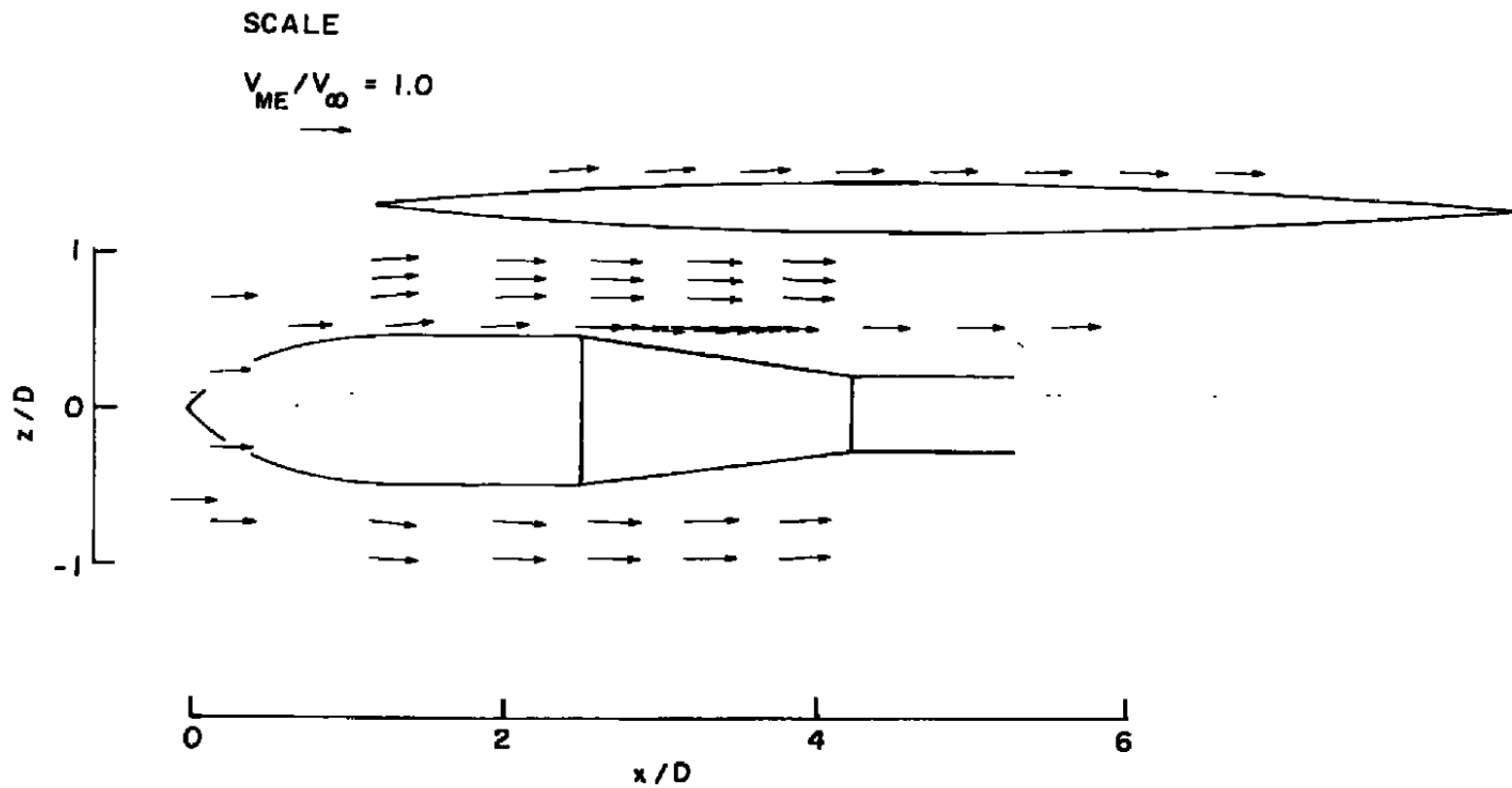
c. Configuration 101  
Figure 14. Concluded.





a. Configuration 122

Figure 15. Effect of pylon on velocity vector projections in constant  $y$  plane for two wing/M-117 configurations ( $\alpha_w = 2.0$ ),  $M_{\infty} = 0.92$ ,  $y/D = 0$ .



b. Configuration 102  
Figure 15. Concluded.

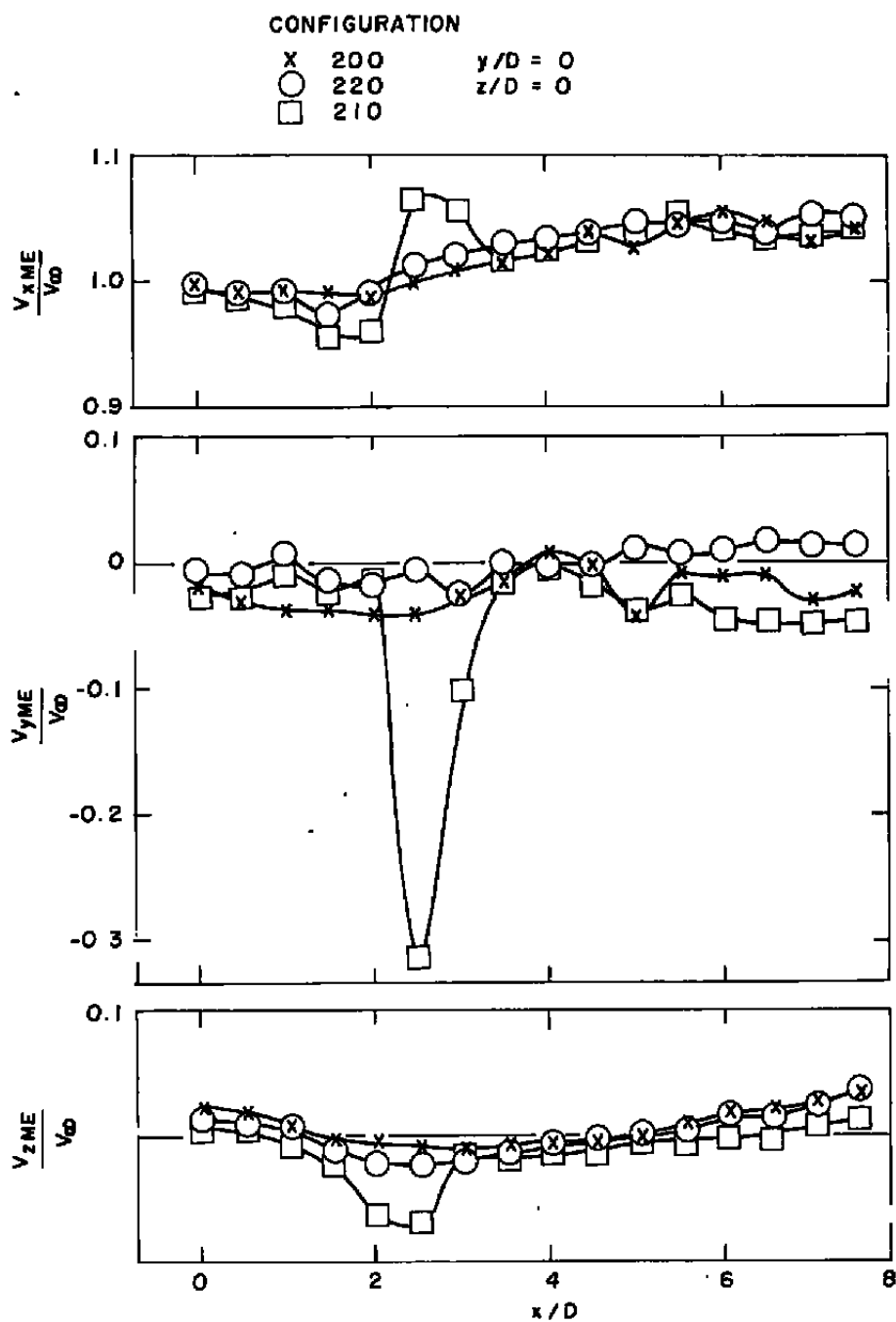
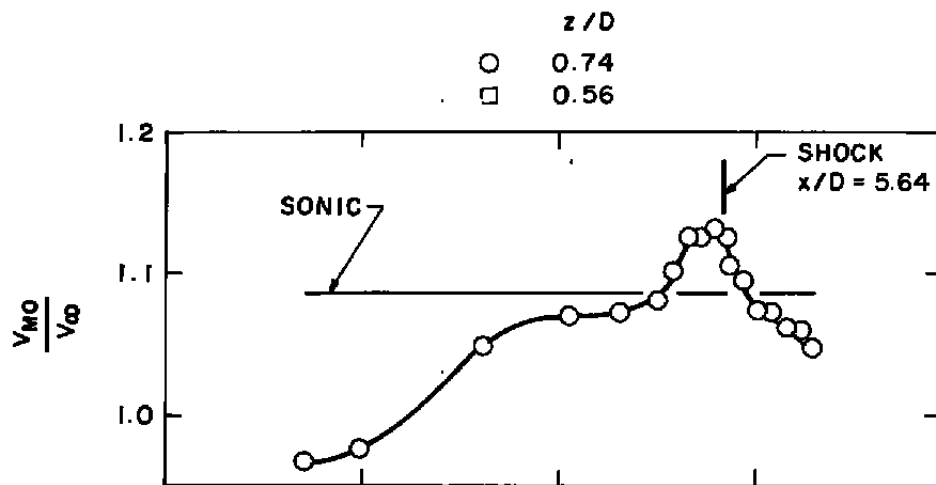
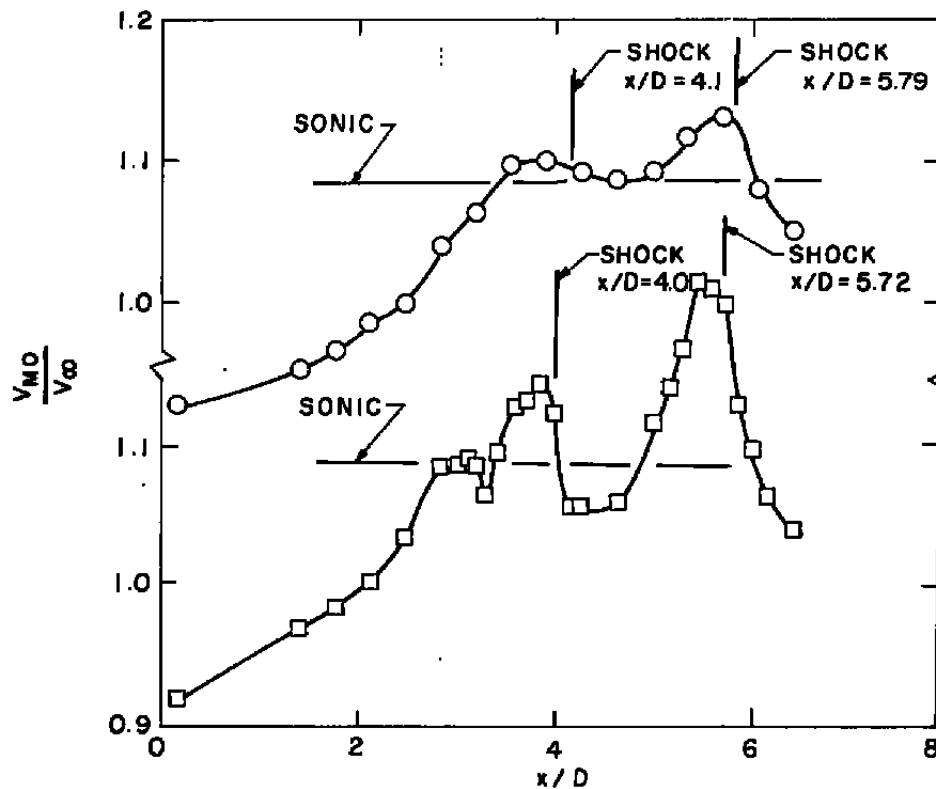


Figure 16. Distribution of the mean velocity components along the x axis (store centerline) with the store removed,  $M_\infty = 0.92$ , Configurations 200, 210, and 220.

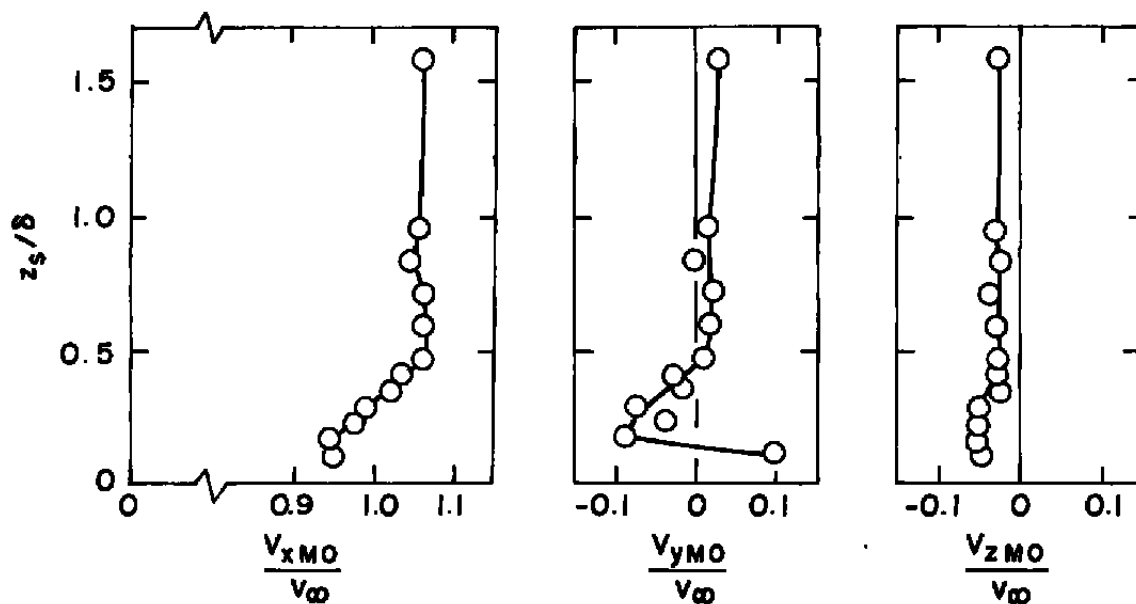


a. Configuration 201

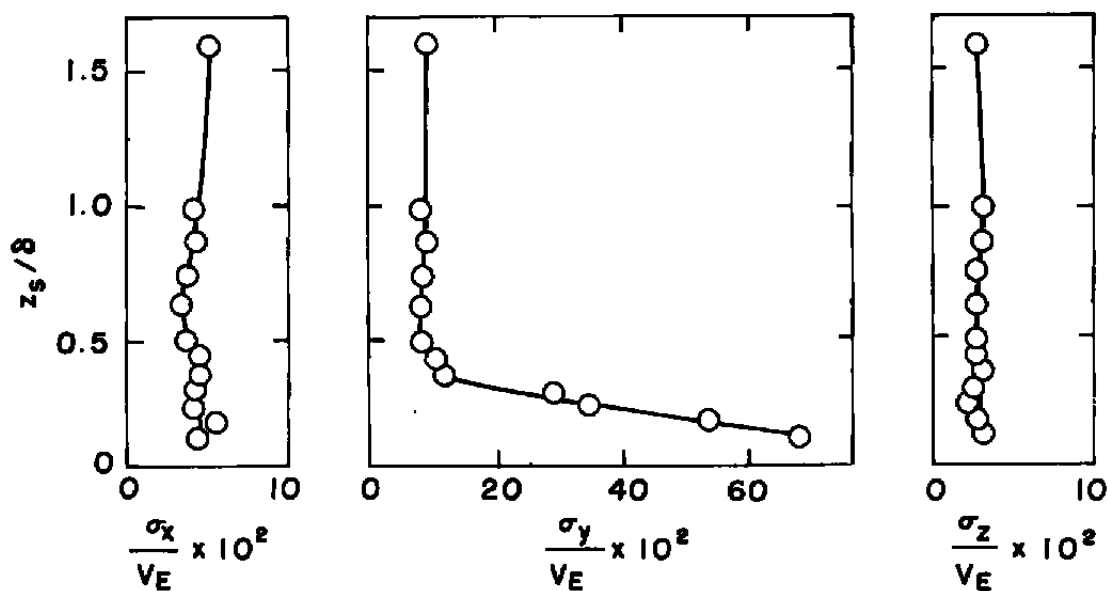


b. Configuration 101

Figure 17. Effect of wing angle on the distribution of mode velocity magnitude between the wing and store,  $M_\infty = 0.92$ ,  $y/D = 0$ .

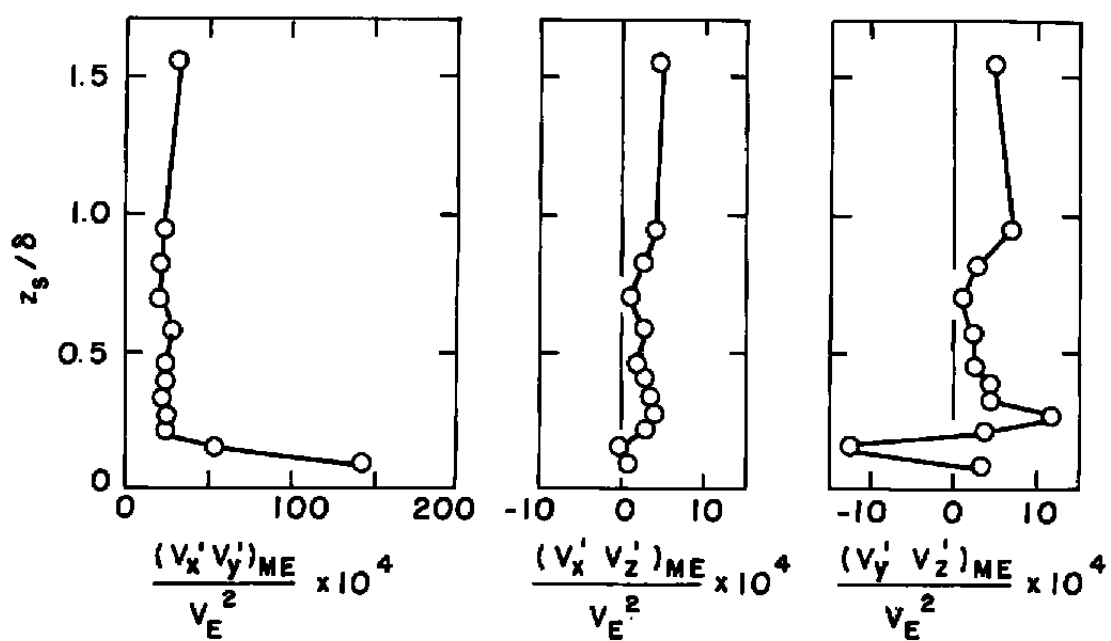


a. Component velocity



b. Turbulent intensity

Figure 18. Wing boundary-layer characteristics on Configuration 100 lower surface,  $M_\infty = 0.92$ .



c. Reynolds shear stress  
Figure 18. Concluded.

Table 1. Definition of Test Configurations

CONFIG	WING		PYLON		STORE		$M_\infty$		
	$\alpha_w = 0$	$\alpha_w = 2.0$	UNSWEPT	SWEPT	MK-83	M-117	0.920	0.975	1.025
221		○		○	○		◇		◇
220		○		○			◇		
201 <sup>*</sup>		○			○		◇		
200 <sup>*</sup>		○					◇		
211		○	○		○		◇		
210		○	○				◇		
121	○			○	○		◇	◇	◇
120	○			○			◇		
101	○				○		◇	◇	
100 <sup>*</sup>	○						◇		
111 <sup>*</sup>	○		○		○		◇		◇
110	○		○				◇		
122	○			○		○	◇		
102	○					○	◇		

\* Configuration convention of Ref. 2 was modified to include pylons and incidence angles.

## Appendix A

### Laser Doppler Velocimeter System Details

The LV shown in Fig. 6 is a differential Doppler system which is further classified as a moving fringe system operating in the backscatter mode. The laser was operated in the all-lines mode at from 6 to 8 w, although the maximum power capability was 18 w. In the all-lines mode the output laser beam actually consists of nine different wavelengths.

The blue (0.488- $\mu\text{m}$  wavelength) and green (0.5145- $\mu\text{m}$  wavelength) beams are the two most powerful of the nine. These two beams were separated from the rest by color filters CF1 and CF2 (Fig. 6). The energy of the seven remaining beams was dissipated by the beam dump, BD. The blue beam was passed through an acousto-optical device termed a dual Bragg cell (Ref. 9), represented in Fig. 6 as the element DBC. The DBC splits the single input beam into four nominally equal power output beams as shown by beam pattern 3, 4, 5, 6 in Fig. 6. Nominally 25 percent of the input beam passes through the DBC and retains its original optical frequency,  $\nu$ , where  $\nu = C/\lambda$ ,  $C$  is the speed of light, and  $\lambda$  is the wavelength of the laser light. Interaction of the input laser beam with acoustic waves in the DBC causes beams 4, 5, and 6 to be split off from beam 3. Interaction with the acoustic waves also causes the optical frequency of beam 4 to shift to  $\nu + 15$  MHz, beam 5 to  $\nu + 60$  MHz, and beam 6 to  $\nu + 45$  MHz. These four beams are projected into the tunnel test section and caused to intersect by lens L9. Lenses L1, L2, and L3 cause the green and blue beams to focus in the intersection region. The diameter of their cigar-shaped intersection regions was about 300  $\mu\text{m}$  for both the blue and green beams.

Beam pairs 3,4 and 5,6 interfere in the intersection region and produce alternate bright and dark fringe planes that move in the x direction at a 15-MHz rate, which is the frequency of the electrical drive signal to the x-axis Bragg cell transducer. A stationary particle in the intersection region scatters light at a 15-MHz rate as the bright fringes sweep past it. A particle traveling in the +x direction scatters light at a rate greater than 15 MHz, whereas a particle traveling in the -x direction scatters light at a rate less than 15 MHz. The moving fringes, therefore, resolve the directional ambiguity problem associated with static fringe LV systems.

The z-axis measurement capability is furnished by beam pairs 3,6 and 4,5, which produce fringes that travel in the -z direction at a rate of 45 MHz. Beam pairs 3,5 and 4,6 also interfere and thereby define diagonal axes with fringes moving at rates of 30 and 60 MHz, but the signals derived from these two axes are later rejected by electronic filtering techniques. Scattered light is collected by lenses L5 and L6 and focused at aperture AP1. Color filter CF3 passes the blue and rejects the green laser light. The photomultiplier tube



PMT1 then produces an electrical signal in response to the scattered blue laser light. The x-axis signal centered at 15 MHz and the z-axis signal centered at 45 MHz are separated by bandpass electronic filters (Ref. 10). Electronic signal processing equipment (Ref. 11) is then used to determine the frequencies of the x-axis and z-axis signals that are proportional to the particle vector component velocities.

The description of the green beam array is similar to that of the blue except that only one Bragg cell is needed to produce the two green beams. Motion of the green fringes is at a 15-MHz rate in the -y' direction. Scattered light is collected by lenses L7 and L8, and the green light is detected by PMT2. The x-y-z velocity components are then derived by transformation from the x-y'-z axis measurements.

The angle subtended by the axes of the transmitted blue and green beams was set at nominally 30 deg, and the angle subtended by a receiver axis and its associated transmitter axis was set at nominally 20 deg. The intersection of the transmitter focal volumes and the receiver image volumes defines the spatial volume from which the scattered light signals originate. This volume is called the probe volume. The dimension of the probe volume in the x and z directions was approximately 300  $\mu\text{m}$  and the dimension in the y direction was approximately 600  $\mu\text{m}$ .

## Appendix B

### Resolution of the y Component of Velocity

The signal frequency produced by one axis of a differential Doppler-type LV system is given by

$$f_D = \frac{1}{2\pi} \vec{V} \cdot (\vec{k}_2 - \vec{k}_1) \quad (B-1)$$

where  $\vec{V}$  is the velocity vector of the light-scattering particle, and  $\vec{k}_1$  and  $\vec{k}_2$  are the propagation vectors of the two intersecting laser beams. From Eq. (B-1) it can be readily seen that an LV system simply measures the orthogonal projection of  $\vec{V}$  onto an axis defined by  $\vec{k}_2 - \vec{k}_1$ . As with the present case, it is oftentimes technically impractical to implement a three-axis LV system in which the three axes are mutually orthogonal. In general, the relationship of the vector components,  $V_i$ , of  $\vec{V}$  referred to the orthogonal, Cartesian, tunnel reference coordinates,  $x_i$ , in terms of the  $(V_\perp)_i$  projections of  $\vec{V}$  onto the oblique, Cartesian coordinates,  $x_i'$ , defined by the LV measurement axes  $i'$ , given by (Ref. 3)

$$\begin{bmatrix} V_1 \\ V_2 \\ V_3 \end{bmatrix} = \frac{1}{\Delta} \begin{bmatrix} (c_{2'2}c_{3'3} - c_{3'2}c_{2'3}) & (c_{3'2}c_{1'3} - c_{1'2}c_{3'3}) & (c_{1'2}c_{2'3} - c_{2'2}c_{1'3}) \\ (c_{3'1}c_{2'3} - c_{2'1}c_{3'3}) & (c_{1'1}c_{3'3} - c_{3'1}c_{1'3}) & (c_{2'1}c_{1'3} - c_{1'1}c_{2'3}) \\ (c_{2'1}c_{3'2} - c_{3'1}c_{2'2}) & (c_{3'1}c_{1'2} - c_{1'1}c_{3'2}) & (c_{1'1}c_{2'2} - c_{2'1}c_{1'2}) \end{bmatrix} \begin{bmatrix} (V_\perp)_{1'} \\ (V_\perp)_{2'} \\ (V_\perp)_{3'} \end{bmatrix} \quad (B-2)$$

where

$$\Delta = c_{1'1}(c_{2'2}c_{3'3} - c_{2'3}c_{3'2}) + c_{1'2}(c_{3'1}c_{2'3} - c_{2'1}c_{3'3}) + c_{1'3}(c_{2'1}c_{3'2} - c_{3'1}c_{2'2}) \quad (B-3)$$

and  $c_{i'j}$  is the cosine of the angle defined by the intersection of the  $x_i'$  and  $x_j$  axes. In the present case

$$c_{1'1} = c_{3'3} = 1 \quad (B-4)$$

and

$$c_{1'2} = c_{1'3} = c_{2'3} = c_{3'1} = c_{3'2} = 0 \quad (B-5)$$

since the  $x_1'$  and  $x_3'$  LV axes are coincident with the  $x_1$  and  $x_3$  tunnel reference axes. Now with more familiar notation where  $x_1 = x$ ,  $x_2 = y$ ,  $x_3 = z$ , and  $x_1' = x'$ ,  $x_2' = y'$ ,  $x_3' = z'$ , Eq. (B-2) becomes

$$\begin{bmatrix} V_x \\ V_y \\ V_z \end{bmatrix} = \begin{bmatrix} 1 & 0 & 0 \\ -\frac{c_{y'x}}{c_{y'y}} & \frac{1}{c_{y'y}} & 0 \\ 0 & 0 & 1 \end{bmatrix} \begin{bmatrix} (V_\perp)_{x'} \\ (V_\perp)_{y'} \\ (V_\perp)_{z'} \end{bmatrix} \quad (\text{B-6})$$

### Appendix C

#### Uncertainty in y Component of Velocity

The overall uncertainty,  $U_f$ , in the determination of a quantity  $f(p_i)$  that is functionally dependent upon various parameters,  $p_i$ , can be expressed by (Refs. 12 and 13)

$$U_f = \pm (B_f + t_{0.95} S_f) \quad (C-1)$$

where  $B_f$  is the overall bias error,  $S_f$  is the overall precision error, and  $t_{0.95}$  is the 95th percentile point for the Student t-distribution. For the degrees of freedom typical of an LV data set,  $t_{0.95} \approx 2.0$ , the overall bias error is defined by

$$B_f = \left[ \sum_{i=1}^n \left( \frac{\partial f}{\partial p_i} b_{p_i} \right)^2 \right]^{1/2} \quad (C-2)$$

where  $b_{p_i}$  is an elemental bias error. Similarly, the overall precision error is related to the elemental precision errors,  $s_{p_i}$ , by

$$S_f = \left[ \sum_{i=1}^n \left( \frac{\partial f}{\partial p_i} s_{p_i} \right)^2 \right]^{1/2} \quad (C-3)$$

The overall uncertainty and repeatability in measurements of a single velocity component obtained with the LV equipment used at AEDC have been previously determined (Refs. 2 and 14). The measurement uncertainty and repeatability in measurement of a single particle velocity in the transonic velocity range should be within  $\pm 1.5$  percent of the recorded value while the uncertainty and repeatability of mean velocity measurements should be within  $\pm 1.3$  percent. However, measurement repeatability fluctuations of several percent were noted whenever the three-component LV system was subjected to varying ambient temperature conditions. Temperature-change-induced movements of the optical elements preceding the two Bragg cells caused changes in the spatial orientation of the beams entering the Bragg cells, ultimately causing small changes in the probe volume fringe spacings (Appendix A). The intensity of the incident laser beams and the low mass and low thermal conductivity of the color filters, CF1 and CF2 (Fig. 6), probably accounted for most of the observed temperature effects. The measurement fluctuations typically subsided to the  $\pm 1$ -percent range after the tunnel and surrounding area reached a stable operating temperature as long as gross air currents in the vicinity of the LV system were suppressed.

With use of Eqs. (C-1), (C-2), and (C-3), an expression for the uncertainty in the determination of the transformed component  $V_y$  can be developed as (with the assumption of uncorrelated elemental errors)

$$U_{V_y} = \pm \left\{ \left[ \left( -\frac{c_{y'x}}{c_{y'y}} \right) s(V_{\perp})_{x'} \right]^2 + \left[ \left( \frac{1}{c_{y'y}} \right) s(V_{\perp})_{y'} \right]^2 + \left[ \left( -\frac{(V_{\perp})_{x'}}{c_{y'y}} \right) s_{c_{y'x}} \right. \right. \\ \left. \left. + \left[ \frac{c_{y'x}(V_{\perp})_{x'} - (V_{\perp})_{y'}}{c_{y'y}^2} \right] s_{c_{y'y}} \right]^2 \right\}^{1/2} \quad (C-4)$$

As might be expected, this expression shows that the uncertainty is a minimum when the  $y'$  axis is coincident with the  $y$  axis and is a maximum when the  $y'$  axis is coincident with the  $x$  axis. For the three-component LV system, the nominal angle subtended by  $y'$  and  $y$  was 120 deg, whereas the angle subtended by  $y'$  and  $x$  was 30 deg with an uncertainty in both angles of  $\pm 0.3$  deg. With use of previously stated uncertainties for  $(V_{\perp})_{x'}$  and  $(V_{\perp})_{y'}$ , Eq. (C-4) for the uncertainty in the determination of  $V_y$  for a single particle from simultaneous  $(V_{\perp})_{x'}$  and  $(V_{\perp})_{y'}$  measurements is

$$U_{V_y} = \pm \left\{ \left[ (0.026)(V_{\perp})_{x'} \right]^2 + \left[ (-0.003)(V_{\perp})_{y'} \right]^2 + \left[ (0.00006)(V_{\perp})_{x'} \right]^2 \right. \\ \left. + \left[ (0.010)(V_{\perp})_{x'} - (0.012)(V_{\perp})_{y'} \right]^2 \right\}^{1/2} \quad (C-5)$$

For small values of  $(V_{\perp})_{y'}$ , the first and last terms are dominant and impart an uncertainty of about  $\pm (0.036)(V_{\perp})_{x'}$  to determinations of  $V_y$ . Thus, the uncertainty amplifying the factor  $(C_{y'x})/(C_{y'y})$  becomes a primary concern when small values of  $(V_{\perp})_{y'}$  are to be measured and when the angles subtended by the  $y'$  and  $y$  axes diverge from 0 or 180 deg and approach 90 or 270 deg, respectively.

Fortunately, because the elemental errors are uncorrelated, the error in mean velocity decreases with increasing sample size. The uncertainty does, however, affect the higher-order statistical parameters since the sample histogram is artificially broadened.

# NOMENCLATURE

$a$	Axial distance from store nose, in. (Fig. 2a)
$B_f$	Overall bias error in determining $f(p_i)$
$b_{p_i}$	Elemental bias error
$C$	Speed of light
$c_i'{}_j$	Cosine of the angle between the $x_i'$ and $x_j$ axes
$D$	Maximum store diameter, in.
$d$	Local store diameter, in. (Fig. 2a)
$e$	Pylon contour coordinate, in. (Fig. 2d)
$f$	Pylon contour coordinate, in. (Fig. 2d)
$f_D$	Doppler frequency
$f(p_i)$	Function dependent upon parameters, $p_i$
$\vec{k}$	Propagation vector of the $i$ th laser beam
$M_\infty$	Free-stream Mach number
$S_f$	Overall precision error in determining $f(p_i)$
$s_{p_i}$	Elemental precision error
$Sta$	Tunnel station, in.
$t$	Half-thickness of wing, in. (Fig. 2c)
$U_f$	Uncertainty in the determination of the function, $f(p_i)$
$\vec{V}$	Velocity vector
$V$	Velocity vector magnitude, ft/sec.
$V_E$	Velocity at boundary-layer edge, ft/sec.
$V_i$	$i$ th component of $\vec{V}$ , ft/sec.
$(V_\perp)_i'$	Projection of $\vec{V}$ onto $x_i'$ axis, ft/sec

$(V_{\perp})_{x'}$	
$(V_{\perp})_{y'}$	Projections of $\vec{V}$ onto $x'$ , $y'$ and $z'$ axis respectively, ft/sec
$(V_{\perp})_{z'}$	
$V_x, V_y, V_z$	$x, y$ , and $z$ components of $\vec{V}$ , ft/sec
$V'_x, V'_y, V'_z$	$x, y, z$ components of perturbation velocity, ft/sec
$V_{\infty}$	Free-stream velocity, ft/sec.
$x, y, z$	Tunnel coordinates, rectangular Cartesian, in.
$x', y', z'$	LV measurement coordinates, oblique Cartesian, in.
$x_i, x_j$	Rectangular Cartesian coordinates ( $i, j = 1, 2, 3$ ), in.
$x_i'$	Oblique Cartesian coordinates ( $i = 1, 2, 3$ ), in.
$x_w$	Chordwise distance from wing leading edge, in. (Fig. 2c)
$z_s$	Cartesian coordinate normal to local surface, in.
$\alpha_s$	Store angle of attack, deg
$\alpha_w$	Angle of incidence between wing and store, deg
$\Delta$	Common denominator in Eq. (B-2)
$\lambda$	Wavelength
$\nu$	Optical frequency
$\sigma_x, \sigma_y, \sigma_z$	Standard deviation of the $V_x, V_y, V_z$ data samples, respectively, ft/sec

**Subscripts**

ME	Mean
MO	Mode

**Abbreviations**

AP	Aperature
BD	Beam dump
CF	Color filter

DBC	Dual Bragg cell
L	Lens
LV	Laser Doppler velocimeter
M	Mirror
PMT	Photomultiplier tube
R	Radius
SBC	Single Bragg cell
W	Window